Combustion and Flame 156 (2009) 588–607

Contents lists available at ScienceDirect

Combustion and Flame

www.elsevier.com/locate/combustflame

Chemical mechanism for high temperature combustion of engine relevant fuels with emphasis on soot precursors

G. Blanquart *, P. Pepiot-Desjardins, H. Pitsch

Department of Mechanical Engineering, Stanford University, Stanford, CA, USA

ARTICLE INFO

Article history:
Received 12 February 2008
Received in revised form 5 December 2008
Accepted 6 December 2008
Available online 17 January 2009

Keywords:
Chemical mechanism
n-Heptane
Iso-octane
Benzene
Acetylene

ABSTRACT

This article presents a chemical mechanism for the high temperature combustion of a wide range of hydrocarbon fuels ranging from methane to iso-octane. The emphasis is placed on developing an accurate model for the formation of soot precursors for realistic fuel surrogates for premixed and diffusion flames. Species like acetylene (C_2H_2), propyne (C_3H_4), propene (C_3H_6), and butadiene (C_4H_6) play a major role in the formation of soot as their decomposition leads to the production of radicals involved in the formation of Polycyclic Aromatic Hydrocarbons (PAH) and the further growth of soot particles. A chemical kinetic mechanism is developed to represent the combustion of these molecules and is validated against a series of experimental data sets including laminar burning velocities and ignition delay times. To correctly predict the formation of soot precursors from the combustion of engine relevant fuels, additional species should be considered. One normal alkane (*n*-heptane), one ramified alkane (iso-octane), and two aromatics (benzene and toluene) were chosen as chemical species representative of the components typically found in these fuels. A sub-mechanism for the combustion of these four species has been added, and the full mechanism has been further validated. Finally, the mechanism is supplemented with a sub-mechanism for the formation of larger PAH molecules up to cyclo[cd]pyrene. Laminar premixed and counterflow diffusion flames are simulated to assess the ability of the mechanism to predict the formation of soot precursors in flames. The final mechanism contains 149 species and 1651 reactions (forward and backward reactions counted separately). The mechanism is available with thermodynamic and transport properties as supplemental material.

1. Introduction

The fuels used both in aircraft (kerosene) and car engines (gasoline and diesel) are composed of a multitude of different molecular components. These components vary in molecular weight and exhibit very different structures. Among these species are linear alkanes such as *n*-heptane (C_7H_{16}), *n*-decane ($C_{10}H_{22}$), branched alkanes such as iso-octane (C_8H_{19}), cyclic alkanes such as cyclohexane (C_6H_{12}), and aromatics such as benzene (C_6H_6), toluene (C_7H_8), or naphthalene (C_8H_{10}). Typical molecules might in fact be complex combinations of different structural groups.

Modeling all the physical and chemical properties of real fuels is challenging as the entire detailed molecular composition of these fuels is not fully known. As a consequence, real fuels are represented typically by surrogates [1,2]. In this approach, a blend of simple hydrocarbon molecules is used, which could reproduce certain physical properties, such as distillation curves and liquid density, or chemical properties, such as ignition delay times, laminar burning velocities, or the formation of pollutants, of the real fuels.

The combustion of fuels such as diesel, gasoline, or kerosene leads to the formation of several kinds of pollutants. Soot particles constitute one of the main pollutants produced in the combustion of these fuels. Past studies have shown the effect of different molecular species on the sooting point [3] or the yield sooting indices [4]. For instance, aromatic molecules such as benzene or toluene are more prone to form soot than alkanes like *n*-heptane or iso-octane.

Modeling soot formation from the combustion of different fuel components generally relies on a detailed chemical mechanism coupled with a soot model [5,6]. These soot models generally assume that the inception of the first soot particles occurs by collision of two Polycyclic Aromatic Hydrocarbons (PAH) [7]. The particles further grow by collision with other particles or by addition of mass onto the surface through chemical reactions [8]. Most models consider that incipient molecules originate in benzene and grow by addition of carbon atoms following the H-abstraction C_2H_2-addition (HACA) mechanism. The same mechanism is usually used to represent the surface reactions. In this framework, benzene molecules are very important as precursors for larger PAHs.

* Corresponding author.
E-mail address: guillaume.blanquart@polytechnique.org (G. Blanquart).

0010-2180/$ – see front matter
doi:10.1016/j.combustflame.2008.12.007

At the same time, acetylene plays a major role as the main component for the growth of both PAH molecules and soot particles. Experimental [4] and numerical [9,10] studies have also suggested the importance of propargyl (C_3H_3) and allyl radicals (C_3H_5) in the formation of benzene and the growth of larger PAH molecules. Understanding the formation mechanisms of these soot precursors from the combustion of real fuels is very important in modeling soot formation.

The purpose of the present work is to develop a single chemical mechanism for the high temperature combustion of both small and larger hydrocarbons while predicting soot precursors with good accuracy. More specifically, the emphasis is placed on the development of a chemical mechanism for realistic fuel surrogates for both premixed and diffusion flames as accurate predictions of soot precursors in these configuration is crucial for predictions of emissions from diesel or jet engines. The mechanism starts with smaller hydrocarbons such as methane (CH_4), acetylene (C_2H_2), ethylene (C_2H_4) and ethane (C_2H_6) as most modeling studies of soot formation have considered these fuels. Additional hydrocarbons such as propyne (C_3H_4), propene (C_3H_6), propane (C_3H_8) and butadiene (C_4H_6) are also considered as their decomposition will lead to radicals involved in the formation of the first aromatic ring (propargyl C_3H_3, allyl C_3H_5 and butadienyl C_4H_5). Finally, two alkanes, one normal (*n*-heptane) and one ramified (iso-octane) as well as two aromatic species (benzene and toluene) are chosen as representative candidates of components found in surrogate fuels.

The article is organized as follows. The first part describes the construction of the chemical mechanism from methane to the four surrogate components. The second part presents a comparison of ignition delay times and laminar burning velocities with experimental data for all fuels considered. Finally, the third part analyzes the formation of soot precursors in several laminar premixed and counterflow diffusion flames.

2. Chemical mechanism

2.1. Mechanism development

The intent of the present work is to develop a consistent chemical mechanism for the combustion of a large number of species ranging from methane (CH_4) up to large hydrocarbon components (C_7H_{16}, C_8H_{18}, ...) typically found in real fuels. In the development of such large chemical models, it is crucial to ensure the self consistency of the rate parameters, the thermochemical data, and the various modeling assumptions. The present chemical model is based on several kinetic mechanisms, each validated for a certain range of species. Unifying these various models requires great care, for the rate parameters and thermochemical data for identical species and reactions can be different.

The chemistry of hydrocarbon species depends strongly upon the chemistry of smaller hydrocarbon molecules but only weakly upon larger species. Based on this observation, the present mechanism was built in several stages, each of these stages corresponding to a given size and type of hydrocarbon molecules. The mechanism is first constructed for small hydrocarbons such as methane (CH_4) and other C_2 fuels. Then, kinetic reactions for larger fuels (C_3 and C_4 species) are added to this mechanism. Finally, the chemistry of aromatic species (benzene and toluene) and large alkanes (*n*-heptane and iso-octane) are included. When incorporating the chemistry of a larger molecule to an existing mechanism, only species and reactions not already present in the mechanism are added. While this procedure does not ensure full consistency between all parameters in the model, it undoubtedly improves both the description of the underlying chemical processes and the predictions from the chemical model.

During the development of the mechanism, it was found that the thermochemical properties of several species needed updates. The properties of some of these species have been recomputed and are presented in the next section. It was also found that the results were very sensitive to several reaction rates. Some of these rates have been updated and are presented in the following sections. In contrary to the thermochemical properties, no reaction rates were recomputed in the present work. When available, the best fit to the most recent experimental data was used. If no experimental data could be found, the reaction products and rate parameters evaluated from high accuracy ab-initio calculations were used. Finally, in some rare cases, when neither experimental nor quantum chemical calculations were available, the rate constants were estimated from similar reactions involving smaller species. No reaction rates have been optimized or arbitrarily changed to match experimental data.

2.2. Thermochemical properties

The thermochemical properties used in the present kinetic mechanism come from various models [22–29]. During the development of the chemical mechanism, it was found that the properties of some species were outdated and that the results showed large sensitivities to the properties for some other species. As a consequence, the thermochemical properties of the most sensitive species have been re-evaluated.

The approach used in the present work follows the methodology used by Blanquart and Pitsch [26] to derive the thermochemical properties of Polycyclic Aromatic Hydrocarbons (PAH). Therefore, only a brief description of the methodology will be presented here. The thermochemical properties of the species have been computed using ab-initio calculations. First, the geometric structures are optimized with B3LYP//6-311++G(d,p). Then, the heat capacity and entropy of formation are computed for these structures. Corrections for hindered rotors are included based on an explicit evaluation of the torsional potential with MP2//cc-pVDZ. Finally, the enthalpy of formation of the different species are evaluated with the hybrid G3MP2//B3 method. When experimental measurements of the enthalpies and/or entropies of formation are available, these values were used in place of the G3MP2//B3 predictions. The G3MP2//B3 predicted values show some systematic errors of a few kJ/mol when compared to the experimental data. Therefore, when no experimental values were available, to improve the predictions of the enthalpy of formation, corrections based on isodesmic reactions were applied as previously done by Wang and Brezinsky [17] for cyclopentadiene derivatives. Table 1 lists the thermochemical properties of the species that were recomputed in the present work.

Among these species, the couple cyclopentadiene/cyclopentadienyl radical plays a significant role. The cyclopentadienyl radical is a typical example of a first-order Jahn–Teller distorted molecule. Two stable C_{2v} conformations with almost the same energy can be found: $^2B_1$ and $^2A_2$. Kiefer et al. [18] and later Tokmakov et al. [19] studied this radical using quantum simulations and estimated the thermodynamic properties of the cyclopentadiene molecule and its radical. A proper consideration of this distortion is necessary to accurately predict the equilibrium constant between the molecule and its radical. For this reason, the thermodynamic properties and the rate constant for the reconversion of cyclopentadienyl into cyclopentadiene were taken from Kiefer et al. [18] (entropy and heat capacity of C_5H_5) and Tokmakov et al. [19] (enthalpy of formation of both C_5H_5 and C_5H_6). These properties were found to have a significant impact on the burning velocities of aromatic species such as benzene.

Table 1
Thermochemical properties of key aromatic species at $T = 298$ K (recomputed quantities in bold). Heat capacity and entropy in J/mol/K and heat of formation in kJ/mol.

Name	Formula	C_p° (298 K)	S° (298 K)	ΔH_f° (298 K)	Source
vinyl oxy radical	CH_2CHO	**53.8**	**259.5**	18.7	Ref. [11]
acetaldehyde	CH_3CHO	**56.1**	**263.1**	−170.7	Ref. [12]
prop-2-vinylidene	C_3H_2	**66.9**	**257.2**	**544.5**	G3MP2B3
2-propynal	C_3H_2O	**63.7**	**275.1**	**126.8**	G3MP2B3
propargyl radical	C_3H_3	**62.9**	**254.6**	339.0	Ref. [13]
allene	A-C_3H_4	**59.1**	**243.3**	190.9	Ref. [12]
propyne	P-C_3H_4	**60.9**	**247.9**	185.4	Ref. [13]
allyl radical (sym.)	A-C_3H_5	**63.4**	**258.6**	166.1	Ref. [14]
allyl radical (sec.)	S-C_3H_5	**65.1**	**271.2**	**271.7**	Iso. Reac.
allyl radical (ter.)	T-C_3H_5	**65.1**	**273.3**	**254.6**	Iso. Reac.
propylene	C_3H_6	**65.1**	**266.8**	19.7	Ref. [12]
butadiynyl radical	C_4H	**58.7**	**249.5**	**826.5**	Iso. Reac.
butadiyne	C_4H_2	**71.9**	**247.6**	46.6	Ref. [15]
i-1-butene-3-yne-2-yl radical	*i*-C_4H_3	**78.7**	**289.1**	499.2	Ref. [15]
e-1-butene-3-yne-2-yl radical	*n*-C_4H_3	**72.2**	**283.6**	547.3	Ref. [15]
1-butene-3-yne	C_4H_4	**72.7**	**283.3**	295.0	Ref. [16]
cyclopentadienone	C_5H_4O	**84.2**	**291.3**	55.2	Ref. [17]
cyclopentadienyl	C_5H_5	**84.5**	265.6	261.5	Refs. [18,19]
cyclopentadiene	C_5H_6	**76.7**	**274.8**	134.3	Ref. [19]
o-benzyne	O-C_6H_4	**81.2**	**284.4**	446.0	Ref. [20]
fulvene	$C_5H_4CH_2$	**91.6**	**294.4**	224.3	Ref. [12]
p-benzoquinone	OC_6H_4O	**109.7**	**325.0**	−115.9	Ref. [21]
benzyl radical	A_1CH_2	**108.4**	**316.6**	207.0	Ref. [13]
toluene	A_1CH_3	**105.4**	**321.5**	50.0	Ref. [13]
benzaldehyde	A_1CHO	**112.1**	**335.9**	−37.2	Ref. [13]
alkoxy-benzyl	A_1CH_2O	**117.0**	**359.9**	**122.4**	Iso. Reac.
cresol radical	OA_1CH_3	**119.2**	**349.1**	**15.2**	Iso. Reac.
indene	C_9H_8	**125.2**	**336.4**	**166.1**	Iso. Reac.
indenyl radical	C_9H_7	**123.6**	**333.4**	**286.1**	Iso. Reac.
indenone	C_9H_6O	**131.9**	**352.1**	**69.3**	Iso. Reac.
1-naphthyl methylene radical	A_2CH_2	**158.7**	**379.0**	**285.1**	Iso. Reac.
1-methylnaphthalene	A_2CH_3	**160.6**	**376.6**	116.9	Ref. [13]

The optimized geometric structures of all species whose thermodynamic properties have been re-evaluated are available as supplemental material.

2.3. Small hydrocarbon chemistry

One of the best models for methane combustion to date is the GRI-MECH v3.0 mechanism [23]. This mechanism already includes C_2 species like acetylene, ethylene and ethane and has been shown to give very good results for combustion of natural gas. However, the burning velocities for species like acetylene and ethylene were not correctly represented. Later, Eiteneer and Frenklach [24] have extended and optimized a larger mechanism based on the GRI-MECH v3.0 for combustion of acetylene. More recently, Davis et al. [22] have reconsidered the combustion of H_2/CO and have developed an optimized mechanism. This mechanism, complemented by the mechanism of Eiteneer and Frenklach [24], is the starting point for the current work.

In the original development of the GRI-MECH v3.0 and in the work of Eiteneer and Frenklach [24] and Davis et al. [22], the mechanisms were optimized in order to improve the comparison with experiments. The Arrhenius prefactors of some reactions were adjusted within the experimental uncertainties to better match a series of targets. In the present work, several new reactions have been added and previously present reactions have been updated with newer experimental or computational evaluation of the rate constants. As a consequence, the rate constants of some of the reactions previously optimized had to be updated. While most of the reactions listed below only lead to a small incremental improvement of the predictions when considered separately, several reactions were found important for configurations such as ignition delay times and laminar burning velocities.

Among these reactions, the reaction of hydrogen recombination with methyl radicals is very important for laminar flame speeds. To improve the overall agreement with experimental measurements, the rate constant for this reaction has been revised. Recently, the high pressure limit rate constant has been evaluated from high-fidelity quantum calculations by Harding et al. [30]. The calculated rate constant has a slight temperature dependence and compares very well with experimental data. The low pressure rate constant was optimized in the successive versions of the GRI-MECH. In the present work, a new fit to experimental measurements for the low pressure rate constant has been derived and used.

To improve the ignition delay times of acetylene, Laskin and Wang [31] considered a new pathway for the activation of acetylene. From quantum calculations, they showed that acetylene can isomerize into singlet vinylidene H_2CC: before reacting with molecular oxygen.

$$C_2H_2 + M \leftrightarrows H_2CC: + M, \tag{1}$$

$$H_2CC: + O_2 \leftrightarrows 3\text{-}CH_2 + CO_2, \tag{2}$$

$$\leftrightarrows 2HCO. \tag{3}$$

Similar analysis has been performed for ethylene [32] at high temperatures. Wang considered the 1,2-H shift in ethylene and the 1,1-H_2 elimination from ethylene to form singlet vinylidene as possible pathways for ethylene activation before reaction with molecular oxygen

$$C_2H_4 + O_2 \rightarrow CH_3 + CO_2 + H, \tag{4}$$

$$C_2H_4 + M \leftrightarrows H_2CC: + H_2 + M. \tag{5}$$

All these reaction pathways have been included in the mechanism and were found important in the prediction of ignition delay times of C_2H_2 and C_2H_4 [32]. Following the work of Laskin and Wang [31], the direct reactions of acetylene and ethylene with oxygen were not included in the mechanism.

The burning velocities of several alkanes, including ethane and *n*-heptane, are very sensitive to the reactions of hydrogen addition

onto acetylene and ethylene to form vinyl and ethyl radicals. These reactions have been recently recomputed with high fidelity quantum calculations by Miller and Klippenstein [33]

$$C_2H_2 + H(+M) \leftrightarrows C_2H_3(+M), \quad (6)$$

$$C_2H_4 + H(+M) \leftrightarrows C_2H_5(+M), \quad (7)$$

and were directly included in the mechanism. The updated rate constants ultimately lead to an increase of the burning velocity for ethane ($\sim$7 cm s^{-1} at $\phi = 1.0$) and *n*-heptane ($\sim$2 cm s^{-1} at $\phi = 1.0$).

Similar quantum calculations have been performed for the reaction of the hydroxyl radical with acetylene and ethylene [34,35]. The reaction with acetylene was found to yield the same products as in the original GRI-MECH,

$$C_2H_2 + OH \leftrightarrows C_2H + H_2O, \quad (8)$$

$$\leftrightarrows HCCOH + H, \quad (9)$$

$$\leftrightarrows CH_2CO + H, \quad (10)$$

$$\leftrightarrows CH_3 + CO. \quad (11)$$

The branching ratios for the four channels are very similar (from 20% to 40%). The reaction with ethylene leads to the formation of the ethoxy radical C_2H_5O in addition to the hydrogen abstraction pathway

$$C_2H_4 + OH \leftrightarrows C_2H_3 + H_2O, \quad (12)$$

$$\leftrightarrows C_2H_5O. \quad (13)$$

This species, which was not included in the original GRI-MECH, is mainly formed at low temperature (below 1000 K), but the branching ratio at moderate temperatures (around 1000 K) remains significant (about 50%). As a result, this species was included in the mechanism. This species can also be formed by O-abstraction from HO_2 by ethyl radical [36]

$$C_2H_5 + HO_2 \leftrightarrows C_2H_5O + OH, \quad (14)$$

or by direct addition of oxygen atoms onto ethyl radicals:

$$C_2H_5 + O \leftrightarrows C_2H_5O. \quad (15)$$

The high pressure limit of the rate constant for this reaction has been calculated by Harding et al. [37]. In the same work, the high pressure rate constants for the oxygen atom addition to methyl and vinyl radicals were also computed. These values were used in the present mechanism. The ethoxy radical can decompose following two pathways [38]

$$C_2H_5O \leftrightarrows CH_3CHO + H, \quad (16)$$

$$\leftrightarrows CH_3 + CH_2O. \quad (17)$$

For high temperature conditions, the reaction rate of the second channel ($CH_3 + CH_2O$) is about twice that of the first channel ($CH_3CHO + H$). Including the formation and consumption pathways of ethoxy radical was also found important during the reduction of the *n*-heptane mechanism (Section 2.7).

The reaction of oxygen atoms with ethylene has been recently analyzed by Nguyen et al. [39]. Three main product channels were considered

$$C_2H_4 + O \leftrightarrows CH_2CHO + H, \quad (18)$$

$$\leftrightarrows 3\text{-}CH_2 + CH_2O, \quad (19)$$

$$\leftrightarrows CH_3 + HCO. \quad (20)$$

The individual rate constants have been fitted between 300 K and 2000 K based on the total rate constant and the individual branching ratios. The branching ratios were found independent upon pressure and of the same order, $\sim$20% for reaction (18), $\sim$25% for reaction (19), and $\sim$45% for reaction (20).

The decomposition of the vinyloxy radical (CH_2CHO) plays a major role in the combustion of C_2 species. Recently, Senosiain et al. [11] calculated the rate constants for the following pathways

$$CH_2CHO \leftrightarrows CH_3 + CO, \quad (21)$$

$$\leftrightarrows CH_2CO + H \quad (22)$$

and found very similar rate constants ($\sim$1:1 branching ratio). In addition to the previous decomposition pathways included in the mechanism, the reaction of oxygen atoms with vinoxy radicals was found to have a very strong sensitivity for several laminar burning velocities. In the GRI-MECH v3.0 [23], the reaction products as well as the rate constant were estimated from the isomeric reaction $CH_3CO + O$

$$CH_2CHO + O \leftrightarrows H + 3\text{-}CH_2 + CO_2. \quad (23)$$

However, the addition of the oxygen atom on the non-terminal carbon atom to form a triradical intermediate ($H_2C\cdot\text{–}CHO\cdot O\cdot$) seems unlikely. Therefore, in the present mechanism, this reaction has been replaced by

$$CH_2CHO + O \leftrightarrows CH_2O + HCO, \quad (24)$$

and the rate constant has been taken from the reaction of oxygen atom with ethyl radical. This change was found to reduce the burning velocities of ethylene by a few cm s^{-1} for lean and stoichiometric mixtures.

Several H-abstraction reactions have also been reconsidered in the light of more recent work. For instance, the rates of the reactions of ethyl radicals with molecular oxygen and methyl radicals were taken from recent quantum simulations [40,41]

$$C_2H_5 + CH_3 \leftrightarrows C_2H_4 + CH_4, \quad (25)$$

$$C_2H_5 + O_2 \leftrightarrows C_2H_4 + HO_2. \quad (26)$$

Miller et al. [40] showed that the reaction of ethyl radicals with molecular oxygen can simply be modeled by the H-abstraction path at high temperatures since the direct addition of O_2 onto the radical occurs only at low temperatures. The rate constant for the H-abstraction channel was evaluated from high quality ab-initio calculation by Miller et al. [40]. This rate is a factor of four smaller than the original rate from the GRI-MECH. Some results such as burning velocities were found to be only weakly sensitive to this rate. However, ignition delay times of *n*-heptane depend strongly on this rate and were found to be too short with the original rate from GRI-MECH.

Most of the H-abstraction reactions from ethane have been updated with more recent values [42–45]

$$C_2H_6 + H \leftrightarrows C_2H_5 + H_2, \quad (27)$$

$$C_2H_6 + OH \leftrightarrows C_2H_5 + H_2O, \quad (28)$$

$$C_2H_6 + HO_2 \leftrightarrows C_2H_5 + H_2O_2, \quad (29)$$

$$C_2H_6 + CH_3 \leftrightarrows C_2H_5 + CH_4. \quad (30)$$

Finally, the ethane decomposition reaction has been reinvestigated recently using shock tube experiments [46]

$$C_2H_6(+M) \leftrightarrows 2CH_3(+M). \quad (31)$$

The new rate constant has been used in the present mechanism.

During the compilation of the chemical mechanism, the reaction rates of a few reactions were found to exceed the collision

limit at room temperature and were therefore updated. However, it was found that the results were insensitive to these changes. For instance, to describe hydrogen abstraction by oxygen atoms on acetylene, the reverse reaction is used with the rate constant recommended by Tsang and Hampson [47]

$$C_2H + OH \leftrightarrows C_2H_2 + O. \quad (32)$$

The recombination rate of the methyl with the formyl radical was estimated to be $k = 5 \cdot 10^{13}$ cm^3 s^{-1} mol^{-1}. Using the reaction equilibrium constant, the backward rate constant can be evaluated and was found to be within the uncertainties of the recommended value of Baulch et al. [45]

$$CH_3 + HCO \leftrightarrows CH_3CHO. \quad (33)$$

2.4. C_3 and C_4 chemistry

While the original GRI-MECH v3.0 already included a skeleton mechanism for combustion of propane, the mechanism did not include the formation of smaller C_3 species like propene (C_3H_6), propyne ($HCCCH_3$) and allene (CH_2CCH_2). The mechanism developed by Eiteneer and Frenklach [24] already includes propene, the C_3H_4 isomers, and most of the high temperature reactions important for C_3 species. This mechanism has been supplemented by a C_4 submechanism taken from Hidaka et al. [48] and Laskin et al. [25]. Some of the reactions have been updated while others have been added to account for more recent data. Only a brief description of the main reactions will be given here.

2.4.1. C_3 chemistry

The formation of C_3 species from small hydrocarbons is considered through a series of reactions. Marinov et al. [49] proposed the methyl addition to acetylene which leads to the formation of both C_3H_4 and C_3H_5 isomers. Later, Davis et al. [50] evaluated the rate parameters for several reactions on the C_3H_5 potential energy surface. More recently, Miller et al. [51] re-evaluated the rate constants using the master-equation methodology for the following reactions

$$C_2H_2 + CH_3 \leftrightarrows p\text{-}C_3H_4 + H, \quad (34)$$

$$\leftrightarrows a\text{-}C_3H_4 + H, \quad (35)$$

$$\leftrightarrows s\text{-}C_3H_5. \quad (36)$$

Given the importance of these pathways for the formation of soot precursors (see Fig. 13), the more advanced quantum calculations of Miller et al. [51] were considered. The rate constants for the first two reactions are only weakly pressure dependent and the rates at $P = 1$ bar were used in the mechanism. For the last reaction, the rate depends strongly on pressure, and thus two rate constants have been included in the mechanism ($P = 1$ bar and $P = 10$ bar). Other product channels were found to be unimportant.

The reaction of acetylene with singlet methylene radicals is another important source of C_3 species. Several quantum calculation [52,53] of this reaction showed that the reaction first leads to the formation of cyclopropene and then allene or propyne, which will ultimately decompose into propargyl radicals

$$C_2H_2 + 1\text{-}CH_2 \leftrightarrows C_3H_3 + H. \quad (37)$$

Blitz et al. [52] measured the reaction rate experimentally. More recently, Yu and Muckerman [53] performed detailed calculations of the reaction and evaluated the rate constant and found only a weak temperature dependence. Thus, the rate used in the mechanism is taken to be constant $k = 1.94 \cdot 10^{14}$ cm^3 mol^{-1} s^{-1}.

In combustion of propene (C_3H_6) in laminar premixed flames, a strong sensitivity of the burning velocities towards the rate of hydrogen recombination with allyl radicals was observed. As a consequence, the rate constant has been re-evaluated. Stoliarov et al. [54] studied the C_3H_6 potential energy surface and considered several reactions

Table 2
Rate coefficients at $P = 1.33$ bar for reactions on the C_3H_6 potential energy surface in Arrhenius form ($k = AT^n \exp(-E/RT)$). Units are cm^3, K, mol, s and kJ.

Reaction	A	n	E	T [K]
$C_3H_6 \leftrightarrows C_2H_3 + CH_3$	$4.04 \cdot 10^{42}$	−7.67	467.90	500–2400
$C_2H_3 + CH_3 \leftrightarrows a\text{-}C_3H_5 + H$	$1.93 \cdot 10^{18}$	−1.25	32.09	500–2400
$a\text{-}C_3H_5 + H \leftrightarrows C_3H_6$	$5.93 \cdot 10^{54}$	−11.76	98.53	900–3000

$$C_3H_6 \leftrightarrows C_2H_3 + CH_3, \quad (38)$$

$$C_2H_3 + CH_3 \leftrightarrows a\text{-}C_3H_5 + H, \quad (39)$$

$$a\text{-}C_3H_5 + H \leftrightarrows C_3H_6. \quad (40)$$

The rate constants for the first two reactions were fitted at $P = 1.33$ bar in the temperature range 500–2400 K. More recently, Harding et al. [55] evaluated the high pressure limit rate constant for the recombination of allyl radical with hydrogen using high fidelity quantum calculations. This rate constant together with the fall-off behavior predicted by Stoliarov et al. [54] was used in the present mechanism. The fitted rate constants for the three reactions are shown in Table 2.

Oehlschlaeger et al. [46] measured from shock tube experiments the rate constant of the propane decomposition to ethyl and methyl radicals

$$C_3H_8(+M) \leftrightarrows C_2H_5 + CH_3(+M), \quad (41)$$

which is used in the present mechanism. Recently, the C_3H_4 potential energy surface has been investigated by Miller and Klippenstein [56]. Three main reactions have been considered and the rate constants from that work are used in the current mechanism

$$C_3H_3 + H \leftrightarrows C_3H_2 + H_2, \quad (42)$$

$$\leftrightarrows p\text{-}C_3H_4, \quad (43)$$

$$\leftrightarrows a\text{-}C_3H_4, \quad (44)$$

$$a\text{-}C_3H_4 \leftrightarrows p\text{-}C_3H_4. \quad (45)$$

These reactions are very important for they describe the conversion of the C_3H_4 isomers into propargyl radicals which would ultimately lead to the formation of the first aromatic ring. The triplet C_3H_2 was found to be the most stable species resulting from the above reactions. During the development of the chemical model, other reactions involving the C_3H_4 isomers were found important. More specifically, the laminar burning velocities of propyne ($p\text{-}C_3H_4$) for rich mixtures ($\phi > 1.2$) and the yield of propyne and allene ($a\text{-}C_3H_4$) in various premixed and diffusion flames are very sensitive to the rates of the following H-abstraction reactions

$$p\text{-}C_3H_4 + H \leftrightarrows C_3H_3 + H_2, \quad (46)$$

$$a\text{-}C_3H_4 + H \leftrightarrows C_3H_3 + H_2, \quad (47)$$

$$p\text{-}C_3H_4 + OH \leftrightarrows C_3H_3 + H_2O, \quad (48)$$

$$a\text{-}C_3H_4 + OH \leftrightarrows C_3H_3 + H_2O. \quad (49)$$

In the absence of direct experimental measurements of these rates, the rate constants for these reactions were taken from similar reactions on ethane (C_2H_6) and ethylene (C_2H_4).

The reaction of propargyl radicals with molecular oxygen has been calculated theoretically by Hahn et al. [57]. Master equation

calculations, in agreement with experiments, suggest that the reaction proceeds as

$$C_3H_3 + O_2 \leftrightarrows CH_2CO + HCO \quad (50)$$

at high temperature. This pathway is one of the major consumption pathways of propargyl radicals and was included in the present chemical model. The reactions of propargyl radicals with other oxygenated species remain unknown and were therefore estimated from similar reactions with acetylene and ethylene. For instance, the following reactions are included in the present mechanism

$$C_3H_3 + OH \leftrightarrows C_2H_3CHO, \quad (51)$$

$$C_3H_3 + OH \leftrightarrows C_2H_4 + CO, \quad (52)$$

$$C_3H_3 + OH \leftrightarrows C_3H_2 + H_2O, \quad (53)$$

$$C_3H_3 + OH \leftrightarrows CH_2O + C_2H_2. \quad (54)$$

2.4.2. C_4 chemistry

Several pathways have been identified producing C_4 species from smaller hydrocarbons. The reaction of addition of ethynyl on acetylene was already included in the mechanism from Eiteneer and Frenklach [24]. Three possible products were considered

$$C_2H_2 + C_2H \leftrightarrows n\text{-}C_4H_3, \quad (55)$$

$$\leftrightarrows i\text{-}C_4H_3, \quad (56)$$

$$\leftrightarrows C_4H_2 + H. \quad (57)$$

The rate constants for the formation of the C_4H_3 isomers showed a strong temperature dependence. Ceursters et al. [58] observed that the addition of ethynyl radicals on acetylene does not exhibit any temperature dependence in the temperature range 295 K $< T <$ 800 K. Furthermore, they found from CCSD(T) calculations that the addition to form n-C_4H_3 is barrier-less, thus justifying the absence of temperature dependence. Therefore, only the addition reaction to form n-C_4H_3 was considered in the present mechanism, and the rate constant measured by Ceursters et al. [58] has been used.

The direct addition of hydrogen atoms onto diacetylene molecules is here described following results from high quality quantum simulations by Miller and Klippenstein [59] for the reactions

$$C_4H_2 + H \leftrightarrows n\text{-}C_4H_3, \quad (58)$$

$$C_4H_2 + H \leftrightarrows i\text{-}C_4H_3. \quad (59)$$

Recently, Senosiain et al. [60] studied the reaction of hydroxyl radical with diacetylene. In addition to the hydrogen abstraction path, they found that the reaction could lead to the formation of two stable species C_3H_3 and C_4H_2O. In the current mechanism, the second minor pathway (C_4H_2O) has been lumped with the first (C_3H_3) as the reaction of decomposition of C_4H_2O are unknown

$$C_4H_2 + OH \leftrightarrows C_4H + H_2O, \quad (60)$$

$$\leftrightarrows C_3H_3 + CO. \quad (61)$$

Reactions of simple radicals (H, OH, O) with diacetylene and vinylacetylene have been updated by considering similar reactions with acetylene and ethylene molecules.

Most of the reactions forming other C_4 species have been updated in light of recent quantum simulations. For instance, Miller et al. [61] studied the reaction of addition of acetylene and vinyl radicals. They found that this reaction proceeds first through the formation of the n-C_4H_5 radicals

$$C_2H_2 + C_2H_3 \leftrightarrows n\text{-}C_4H_5. \quad (62)$$

Table 3
Rate coefficient for the recombination of cyclopentadienyl radicals in Arrhenius form ($k = AT^n \exp(-E/RT)$). Units are cm^3, K, mol, s and kJ.

Reaction	A	n	E
$C_5H_5 + C_5H_5 \leftrightarrows C_{10}H_8 + 2H$	$6.39 \cdot 10^{29}$	−4.03	147.30

The reaction rate they evaluated was used in the present mechanism. This reaction was found very important in predicting the laminar burning velocities of butadiene (C_4H_6) and benzene (C_6H_6). The reaction of vinyl addition onto ethylene has been studied by Shestov et al. [62]

$$C_2H_4 + C_2H_3 \leftrightarrows 1,3\text{-}C_4H_6 + H. \quad (63)$$

The rates of reaction computed from quantum calculations have been used for these two reactions.

Finally, the reactions of molecular oxygen with butadienyl radicals were derived from similar reactions with vinyl radical

$$n\text{-}C_4H_5 + O_2 \leftrightarrows C_4H_4 + HO_2, \quad (64)$$

$$\rightarrow a\text{-}C_3H_5 + CO + O, \quad (65)$$

$$\leftrightarrows HCO + C_2H_3CHO, \quad (66)$$

$$i\text{-}C_4H_5 + O_2 \leftrightarrows C_4H_4 + HO_2. \quad (67)$$

2.5. Aromatic chemistry

A base mechanism for combustion of aromatic species has been derived from the work of Djurisic and Wang [63,64] for the oxidation of benzene, the work of Zhong and Bozzelli [65,66] for the oxidation of cyclopentadiene, and the work of Oehlschlaeger et al. [67] for the oxidation of toluene.

2.5.1. Cyclopentadiene chemistry

Most of the reactions for the chemistry of cyclopentadiene were taken from the work of Zhong and Bozzelli [65,66]. However, some key reactions for the cyclopentadiene pyrolysis have been updated. The rate for the reactions of hydrogen atoms with cyclopentadiene were taken from Roy and Just [68]

$$C_5H_6 + H \leftrightarrows C_5H_5 + H_2, \quad (68)$$

$$C_5H_6 + H \leftrightarrows a\text{-}C_3H_5 + C_2H_2. \quad (69)$$

The rate for the recombination of propargyl radicals with acetylene molecules was taken from Knyazev and Slagle [69]

$$C_3H_3 + C_2H_2 \leftrightarrows C_5H_5. \quad (70)$$

The recombination of cyclopentadienyl radicals leading to the formation of naphthalene was originally proposed by Marinov et al. [49]

$$C_5H_5 + C_5H_5 \rightarrow C_{10}H_8 + 2H. \quad (71)$$

This scheme has been the subject of several studies [70–72], but no consensus is available for the rate constant of the reaction. Recently, this reaction has been studied both experimentally [73] and numerically [74]. Kislov and Mebel [74] found that this reaction leads to the formation of naphthalene at low temperatures and fulvalene at high temperatures. Their branching ratio together with the total rate constant from Murakami et al. [73] has been used to evaluate the rate constant of naphthalene formation (Table 3). This new rate constant is used in the present work for the naphthalene pathway which is of key importance for larger PAH formation. The combination of the total rate constant of Murakami et al. [73] and the branching ratios of Kislov and Mebel [74] was found necessary to reproduce the concentration of naphthalene in cyclopentadiene pyrolysis in plug flow reactors [75] (results not shown here).

The oxidation of cyclopentadiene leads to the formation of several intermediate species like cyclopentadienoxy radicals (1,3-C_5H_5O and 2,4-C_5H_5O), cyclopentadienone (C_5H_4O), and vinyl ketene (C_4H_4O). Reaction rates for those species were estimated from similar reactions with smaller hydrocarbon molecules.

2.5.2. Benzene chemistry

In the current mechanism, the formation of benzene molecules occurs following two pathways. The first pathway, originally investigated by Wang and Frenklach [76], corresponds to the acetylene addition onto C_4H_3 or C_4H_5 radicals. In certain flames, such as the acetylene diffusion flame discussed in Section 4.2, these pathways can represent about half of the total formation rate of benzene. Therefore, it is important to include the best description of the rate constants. Recently, high fidelity ab-initio calculations for this reaction have been performed by Senosiain and Miller [77] on the acetylene addition onto the C_4H_5 isomers. The reaction with n-C_4H_5 was found to produce mainly benzene and fulvene ($C_5H_4CH_2$)

$$n\text{-}C_4H_5 + C_2H_2 \leftrightarrows C_5H_4CH_2 + H, \quad (72)$$

$$\leftrightarrows C_6H_6 + H, \quad (73)$$

while the reaction with i-C_4H_5 was found to produce mainly fulvene

$$i\text{-}C_4H_5 + C_2H_2 \leftrightarrows C_5H_4CH_2 + H. \quad (74)$$

Other linear C_6H_6 molecules are formed during these reactions especially at higher temperatures ($T > 2000$ K) but were not considered in the present mechanism. These reaction rates are several times larger than the original values from Wang and Frenklach [76] and were found very sensitive for the production of the first aromatic ring in an acetylene rich environment. The reactions of acetylene with the C_4H_3 isomers were taken from Wang and Frenklach [76].

The second pathway towards the formation of benzene molecules is the self-recombination of propargyl radicals (C_3H_3) or the reaction of propargyl radicals with allyl radicals (a-C_3H_5). These resonantly stabilized free radicals (RSFR) are usually found in significant concentrations in flames. Miller and Klippenstein [9] studied the C_6H_6 potential energy surface and found the following reactions to be important

$$C_3H_3 + C_3H_3 \leftrightarrows C_5H_4CH_2, \quad (75)$$

$$\leftrightarrows C_6H_6, \quad (76)$$

$$\leftrightarrows C_6H_5 + H, \quad (77)$$

$$C_5H_4CH_2 \leftrightarrows C_6H_6, \quad (78)$$

$$\leftrightarrows C_6H_5 + H. \quad (79)$$

More importantly, they found that the recombination rate is not constant with temperature as usually assumed but rather decreases with increasing temperature. Recently, Georgievskii et al. [78] computed the association rate constant for the reaction of propargyl recombination using high fidelity quantum calculations. In the present mechanism, the rate constants are evaluated from the branching ratios listed in [9] and the total rate constant given in [78].

One additional molecule, the 2-ethynyl-1,3-butadiene, was found important [9]. However, this species isomerizes quickly into fulvene. Thus, its reaction of formation has been lumped with that of fulvene.

Finally, the reaction of propargyl with allyl radicals is assumed to follow

$$C_3H_3 + a\text{-}C_3H_5 \leftrightarrows C_6H_6 + H_2. \quad (80)$$

Table 4
Rate coefficients for the formation of the first aromatic ring from the recombination of resonantly stabilized radicals in Arrhenius form ($k = AT^n \exp(-E/RT)$). Units are cm^3, K, mol, s and kJ.

Reaction	P [bar]	A	n	E
$C_3H_3 + C_3H_3 \leftrightarrows C_5H_4cH_2$	1	$8.25 \cdot 10^{46}$	−10.10	70.96
	10	$5.53 \cdot 10^{42}$	−8.77	66.38
$\leftrightarrows C_6H_6$	1	$1.07 \cdot 10^{45}$	−9.57	71.19
	10	$7.17 \cdot 10^{40}$	−8.24	66.61
$\leftrightarrows C_6H_5 + H$	1	$5.77 \cdot 10^{37}$	−7.00	131.82
	10	$3.87 \cdot 10^{33}$	−5.67	127.24
$a\text{-}C_3H_5 + C_3H_3 \leftrightarrows C_6H_6 + H_2$	1	$1.64 \cdot 10^{44}$	−9.20	63.40
	10	$1.10 \cdot 10^{40}$	−7.87	58.82

Georgievskii et al. [78] evaluated the high pressure limit of the association reaction. The reaction is assumed to exhibit the same pressure fall-off behavior as for propargyl self-recombination. As a result, the reaction rate at atmospheric pressure is evaluated using the high pressure limit for reaction (80) and the ratio of atmospheric to high pressure rates for the reaction $C_3H_3 + C_3H_3$. The rates for reactions (75)–(80) at $P = 1$ bar and $P = 10$ bar are listed in Table 4. However, these rate constants are most likely overestimated as they do not account for the slow chemical conversion of C_6H_8 species into a C_6H_6 species. Furthermore, during the validation of the present model with experimental data, these rate constants were found to lead to the formation of an excess of benzene molecules. Reducing the rate constants for the recombination of allyl and propargyl radicals by a factor of two was found to lead to better comparison with experimental data. While this reduced rate has been used in the present mechanism, further analysis of this reaction should be considered.

The base mechanism for the oxidation of benzene was taken from the work of Djurisic and Wang [63]. Several reactions have been changed and updated in light of newer experimental measurements or ab-initio calculations. For instance, the reactions of benzene with OH radicals have been investigated by Tokmakov and Lin [79] and Seta et al. [80]

$$C_6H_6 + OH \leftrightarrows C_6H_5 + H_2O, \quad (81)$$

$$\leftrightarrows C_6H_5OH + H. \quad (82)$$

The rate for oxygen addition to benzene is assumed to follow two pathways

$$C_6H_6 + O \leftrightarrows C_6H_5O + H, \quad (83)$$

$$\leftrightarrows C_6H_5OH. \quad (84)$$

Other products such as $C_5H_5 + HCO$ and $C_5H_6 + CO$ have been considered in previous studies of this reaction [81,82]. However, recent quantum chemical calculations suggest that these pathways are marginal or unimportant under the present temperature and pressure conditions [83]. The total rate constant has been taken from Nguyen et al. [83], but the branching ratio between the two pathways (reactions (83) and (84)) is not known. Therefore, equal branching ratio was assumed between the two pathways as suggested by Baulch et al. [45]. The reaction of decomposition of phenol has been investigated by Xu and Lin [84]

$$C_6H_5OH \leftrightarrows C_6H_5O + H, \quad (85)$$

$$\leftrightarrows C_5H_6 + CO \quad (86)$$

and is used here. Finally, the rate of phenoxy radical decomposition is taken from the experimental study by Murakami et al. [85]

$$C_6H_5O \leftrightarrows C_5H_5 + CO. \quad (87)$$

2.5.3. Toluene chemistry

The base mechanism for toluene oxidation has been derived from the work of Oehlschlaeger et al. [67]. Some reactions have been updated to account for newer results. For instance, the reaction of toluene decomposition has been recently studied by Klippenstein et al. [86]

$$C_6H_5CH_3 \leftrightarrows C_6H_5 + CH_3, \quad (88)$$

$$\leftrightarrows C_6H_5CH_2 + H, \quad (89)$$

$$C_6H_5CH_2 + H \leftrightarrows C_6H_5 + CH_3. \quad (90)$$

The formation of benzyl radicals was found to be between two and three times faster than the formation of phenyl radicals.

As benzyl radicals are resonantly stabilized radicals, they are found in large concentrations in flames. As a result, it is important to accurately describe both their formation and their decomposition. While the rate of the decomposition reaction has been measured recently by Oehlschlaeger et al. [87], the product distribution is not fully known. Several possible products have been suggested in the literature for the decomposition of benzyl radical [87,88] such as cyclopentadienyl radical plus acetylene, vinylacetylene (C_4H_4) plus propargyl, or a linear C_7H_6 molecule. Ab-initio calculations [88] suggest that the pathway leading to the formation of cyclopentadienyl is certainly one of the most important. Furthermore, the reaction of acetylene addition onto cyclopentadienyl radicals was found to produce a C_7H_7 radical [69]. Therefore, in the current mechanism, benzyl is assumed to decompose as

$$C_6H_5CH_2 \leftrightarrows C_5H_5 + C_2H_2. \quad (91)$$

As a resonantly stabilized free radical (RSFR), the benzyl radical is very stable and is found in significant concentration in flames. Furthermore, its chemical structure is very similar to that of allyl radicals. As suggested by McEnally et al. [72], benzyl radicals can react with propargyl to form naphthalene

$$C_6H_5CH_2 + C_3H_3 \rightarrow C_{10}H_8 + H_2. \quad (92)$$

The real product of the above reaction should be a $C_{10}H_{10}$ species. Through H-abstraction reactions, this molecule is assumed to transform into naphthalene. The rate of the reaction of allyl radicals with propargyl has been used for this reaction. This pathway was found to be a significant source of naphthalene molecules.

Other reactions relevant to the oxidation of toluene have been updated. The reaction of OH radical with toluene is assumed to follow three pathways

$$C_6H_5CH_3 + OH \leftrightarrows C_6H_5CH_2 + H_2O, \quad (93)$$

$$\leftrightarrows HOC_6H_4CH_3 + H, \quad (94)$$

$$\leftrightarrows C_6H_5OH + CH_3. \quad (95)$$

The rate for H-abstraction from the methyl group of toluene has been taken from Vasudevan et al. [89], while the H and CH_3-substitution rates were taken from Seta et al. [80]. Among these pathways, the H-abstraction from the methyl group is much faster ($\sim$10 times) than the substitutions.

Recently, Choi et al. [90] and Xia and Lin [91] studied the decomposition of the $C_6H_5CH_2O$ radical on the C_7H_7O potential energy surface and considered the following reactions

$$C_6H_5CH_2O \leftrightarrows C_6H_5CHO + H, \quad (96)$$

$$C_6H_5 + CH_2O \leftrightarrows C_6H_6 + HCO, \quad (97)$$

$$\leftrightarrows C_6H_5CHO + H, \quad (98)$$

$$\leftrightarrows C_6H_5CH_2O. \quad (99)$$

Rates derived by ab-initio calculations were used in the present mechanism. These rates were evaluated at different pressure than atmospheric pressure. However, the present results were found to be marginally dependent upon the rate constants, and no additional evaluation of the rate constants for atmospheric combustion was performed. The rates for the reaction of C_6H_5CHO were taken from similar reactions with CH_3CHO. Finally, cresol molecules were considered and the rates for the relevant reactions were taken from the chemistry of benzene and phenol molecules.

2.6. Large PAH chemistry

In order to be used in soot models, the kinetic scheme is supplemented by a mechanism for the growth of Polycyclic Aromatic Hydrocarbon (PAH) molecules beyond benzene. This mechanism is based on several reaction pathways. The first path corresponds to the HACA mechanism [8]. Aromatic rings composed of six carbon atoms are formed from the successive addition of two acetylene molecules. The rate of acetylene addition on a radical molecule like phenyl or naphthyl is taken from Kislov and Mebel [92]. The second path is the addition of propargyl radicals on substituted aromatic molecules [10,72]. For instance, naphthalene can be formed by the addition of propargyl on a benzyl radical. The rate of propargyl addition is taken from Miller and Klippenstein [9] and Georgievskii et al. [78] as was done for similar reactions with C_3H_3 and a-C_3H_5. The third path is the addition of vinylacetylene (C_4H_4) on an aromatic radical followed by direct cyclization [93,94]. The channel entrance rate computed by Aguilera-Iparraguirre and Klopper [94] has been used in the mechanism. Finally, the last reaction pathway corresponds to the recombination of cyclopentadienyl radicals to form naphthalene or the reaction of cyclopentadienyl and indenyl radicals to form phenanthrene [10]. The thermodynamic properties for the different PAH molecules up to cyclo[cd]pyrene were taken from the recent compilation of Blanquart and Pitsch [26]. Some of the reaction rates leading to the formation of large PAH molecules are pressure dependent. For this reason, the present mechanism includes rate constants at two nominal pressures, $P = 1$ bar and $P = 10$ bar, when necessary.

2.7. n-Heptane and iso-octane chemistry

The description of the *n*-heptane and iso-octane combustion chemistry has been taken from the Lawrence Livermore National Laboratories (LLNL) mechanisms developed for *n*-heptane by Curran et al. [27] and for iso-octane by Curran et al. [28]. However, these mechanisms are very large and include many species and reactions relevant to the low temperature oxidation of hydrocarbons that are not important for the high temperature conditions considered in this work. To remove the low temperature chemistry and negligible chemical paths, both the *n*-heptane and iso-octane mechanisms were reduced independently using the DRGEP method developed by Pepiot-Desjardins and Pitsch [95]. Reduction was performed for the homogeneous, isochoric, and adiabatic autoignition of mixtures of fuel and air, for temperatures between 1000 and 2000 K, pressures between 1 and 40 bar, and equivalence ratios ranging from 0.5 to 2. The targets used for the reduction included the ignition delay time, fuel, oxidizer, and main combustion products. The DRGEP reduction procedure was complemented by appropriate species and reactions lumping, guided by a thorough reaction flux analysis.

Because the resulting skeletal mechanisms have species and reactions in common that are already included in the mechanism developed in the previous sections, the schemes must be combined carefully. The following rules were applied: Any species or reactions not already present in the current mechanism were simply added. Additionally, when identical reactions were available,

the reactions of the current mechanism were preferred over the reactions from the skeletal LLNL mechanisms. The resulting final mechanism consists of 149 species and 1651 reactions, forward and backward reactions being counted separately, of which 14 species and 84 reactions come from the *n*-heptane LLNL mechanism and 14 species and 73 reactions from the iso-octane LLNL mechanism.

3. Validation results

Laminar burning velocities and ignition delay times were chosen as targets for the validation of the presented chemical mechanism. The combination of these data provides a good test for the developed mechanism. These two cases also represent possible modes of combustion often found in engines: flame front propagation and local thermal ignition. In addition, in the next section, species profiles are compared with experiments for a series of premixed and diffusion flames.

Note that, although the low temperature auto-ignition chemistry has been neglected and consequently will not be tested here, it is still possible to extend the present mechanism by including appropriate reactions from the LLNL detailed chemical schemes. All numerical simulations have been performed with the FlameMaster code V4.0 [96].

3.1. Ignition delay times

In order to validate the mechanism over a large range of equivalence ratios, auto-ignition simulations, modeled by isochoric and adiabatic homogeneous reactors, are performed for lean ($\phi = 0.5$), stoichiometric ($\phi = 1.0$), and rich ($\phi = 2.0$) mixtures for conditions and fuels for which experimental data are available. In the numerical simulations, ignition was defined by the location of the maximum temperature gradient, unless specifically noted. Most of the simulations were done around atmospheric pressure, with the exception of those for *n*-heptane and iso-octane which were done at much higher pressures (up to 40 bar). When several experimental data sets exist for the same equivalence ratio and pressure, the most recent data set is used.

3.1.1. Small hydrocarbons

The experimental data for the ignition delay times of small hydrocarbons were taken from Seery and Bowman [97] for methane combustion, from Hidaka et al. [98] ($\phi = 2.0$) and Rickard et al. [99] ($\phi = 0.5$ and $\phi = 1.0$) for acetylene combustion, from Hidaka et al. [100] ($\phi = 0.5$ and $\phi = 2.0$) and Horning [101] ($\phi = 1.0$) for ethylene combustion, and from de Vries et al. [102] for ethane combustion. The ignition delay times for the case of ethane were evaluated numerically as the onset of OH and CH increase as it was defined in the experimental setup of [102].

Fig. 1 shows the ignition delay times for the small hydrocarbons predicted with the current mechanism. For methane, acetylene, and ethylene, the ignition delay times compare very well with the experimental data. On the other hand, the computed ignition delay times for ethane show slight deviations from the experimental measurements. The ignition delay times predicted with the current mechanism for the lean case ($\phi = 0.5$) are smaller than measured experimentally. However, the experimental measurements suffer from some scatter, and the overall prediction remains very good.

3.1.2. C_3 and C_4 species

The experimental data for the ignition delay times for C_3 and C_4 species are taken from Curran et al. [103] for propyne and allene combustion, from Qin et al. [104] for propene combustion, from Brown and Thomas [105] ($\phi = 1.0$) and Burcat et al. [106] ($\phi = 0.5$ and $\phi = 2.0$) for propane combustion, and from Libby et al. [107] ($\phi = 0.5$ and $\phi = 1.0$) and Fournet et al. [108] ($\phi = 1.38$) for butadiene combustion. The ignition delay times for lean and rich propane as well as for rich butadiene mixtures were performed at a slightly higher pressure than the other simulations ($P \approx 10$ bar).

Fig. 2 shows the ignition delay times predicted with the current mechanism. In spite of a short chemical mechanism for the combustion of the C_3 and C_4 species, the comparison of the results of the numerical simulations with the experimental values is very good in almost all cases. However, butadiene ignition at high pressure ($P = 10$ bar) and rich mixtures shows some errors. Similar errors were also found by Laskin and Wang [25]. They concluded that the butadiene ignition data of Fournet et al. [108] are potentially erroneous, due to an inaccurate calculation of the temperature behind reflected shock waves. Another source of error might come from using rate constants derived from quantum calculations at atmospheric pressure [109]. While these rate constants might be inaccurate for higher pressures, they should be revisited once new experimental data confirm the measurements of Fournet et al. [108].

3.1.3. Aromatics

Experimental data for the ignition delay times for the two aromatic species are taken from Burcat et al. [110] for benzene combustion and from Burcat et al. [110] ($\phi = 0.33$ and $\phi = 1.0$) and Dagaut et al. [111] ($\phi = 1.5$) for toluene combustion.

Fig. 3 shows the ignition delay times predicted with the current mechanism. For both benzene and toluene, the ignition delay times for stoichiometric mixtures are in excellent agreement with the experimental measurements. However, there are some errors for lean and rich mixtures. Lean mixtures tend to ignite too late while rich mixtures tend to ignite too early. Although the model correctly captures the trend of increasing ignition delay times for richer mixtures, this dependance is found to be too weak for the present chemical scheme. Since toluene exhibits the same tendency as benzene, one could stipulate that these discrepancies originate in the description of the reactions on the aromatic ring. Given the large experimental uncertainties in several key reactions and the lack of conclusive ab-initio calculations, the present results remain very good (less than 50% relative error for lean and rich mixtures).

3.1.4. n-Heptane and iso-octane

The experimental data for the ignition delay times of *n*-heptane were taken from Ciezki and Adomeit [112] and Gauthier et al. [113]. The ignition delay times of Gauthier et al. [113] were rescaled to $P = 3.2$ bar, $P = 13.5$ bar, and $P = 42$ bar as suggested in Ref. [113]. For iso-octane, the data were taken from Fieweger et al. [114] and Davidson et al. [115].

Fig. 4 shows the ignition delay times predicted with the current model and with the original chemical mechanisms from Curran et al. [27,28]. Since the *n*-heptane and iso-octane chemistry of the current mechanism comes from the LLNL mechanisms, the ignition delay times are expected to be very close to those predicted with the detailed LLNL mechanisms. However, as the low temperature chemistry was removed during the chemical reduction, the numerical simulations should only be compared to the experimental measurements at high temperature.

As expected, the ignition delay times for iso-octane combustion are in close agreement with those predicted with the detailed LLNL mechanism. Furthermore, the comparison with experimental measurements is very good. Similar conclusions can be drawn for heptane combustion. For lean mixtures, the ignition delay times predicted with the current mechanism and the LLNL mechanism are about the same. As the equivalence ratio increases, the differences between the two mechanisms increase. It should be noted that these differences arise from the combination of the *n*-heptane and

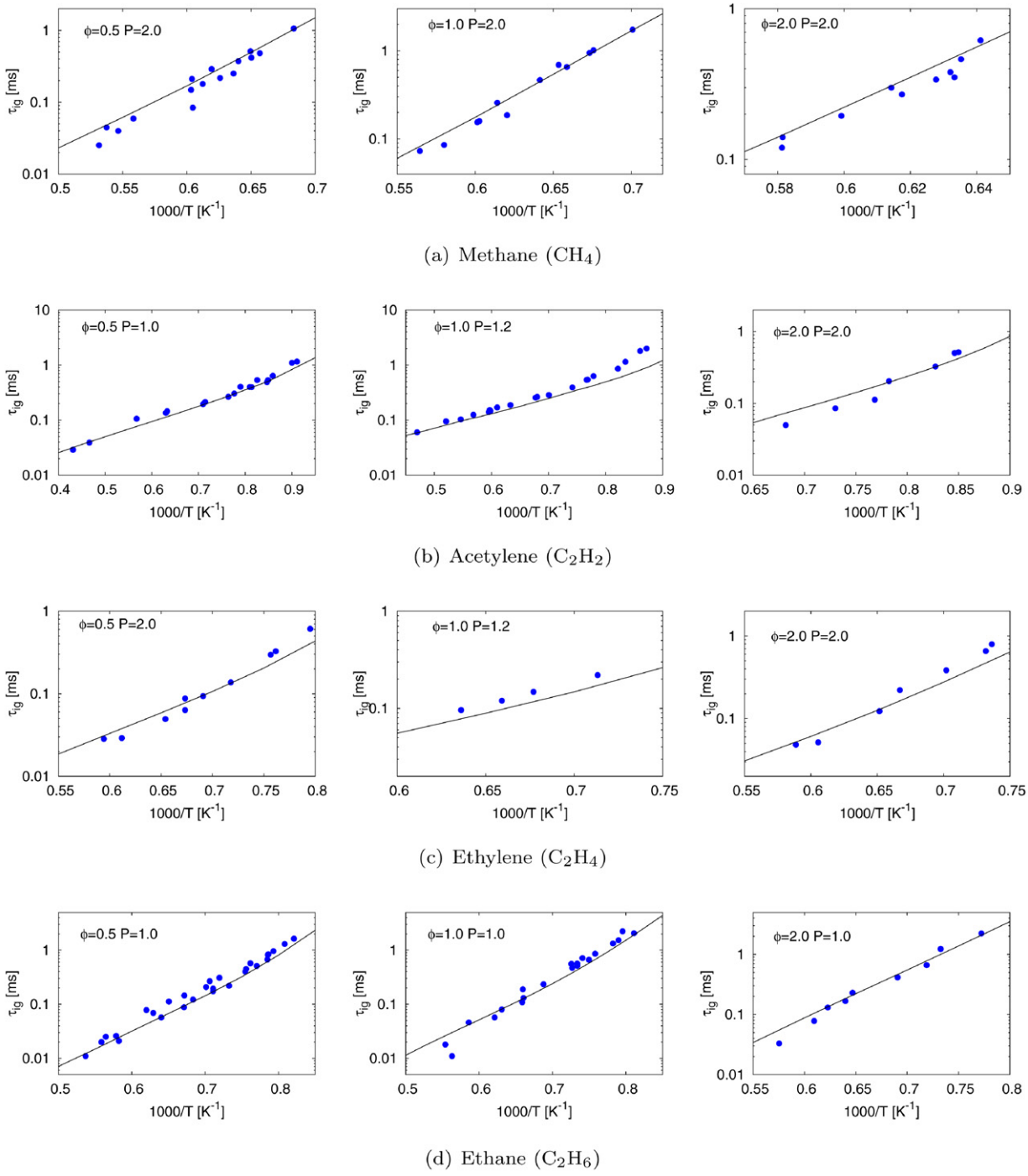

Fig. 1. Ignition delay times for small hydrocarbons. References for experimental data are given in the text.

iso-octane mechanisms with a different base scheme and not from the reduction of the original mechanisms. The current mechanism predicts ignition delay times usually lower than the LLNL mechanism. However, these predictions are closer to the experimental measurements, and the error is hence within the predictive accuracy of the original mechanism. At low temperatures, $T < 1000$ K for *n*-heptane and $T < 1100$ K for iso-octane, the experimental data start to show a negative temperature coefficient (NTC) behavior. This behavior is not captured by the present mechanism as the low temperature chemistry has been omitted. Furthermore, at these low temperatures, the prediction of ignition delay might be affected by non-ideal effects [116], thus partially explaining the differences between experimental and numerical results.

3.2. Laminar burning velocities

3.2.1. Numerical methods

Laminar burning velocities were computed numerically for all fuels for which experimental data are available and compared to measurements. The laminar burning velocities were evaluated as the eigenvalue of a system of 1D ordinary differential equations describing an adiabatic unstretched premixed flat flame [96]. Soret and Duffour effects were included in the calculations as well as recent improvements in the evaluation of the diffusion coefficients of H and H_2 [117,118]. Because of the large size of the chemical mechanism, multicomponent transport properties could not be used and were replaced by mixture averaged properties as described in [96].

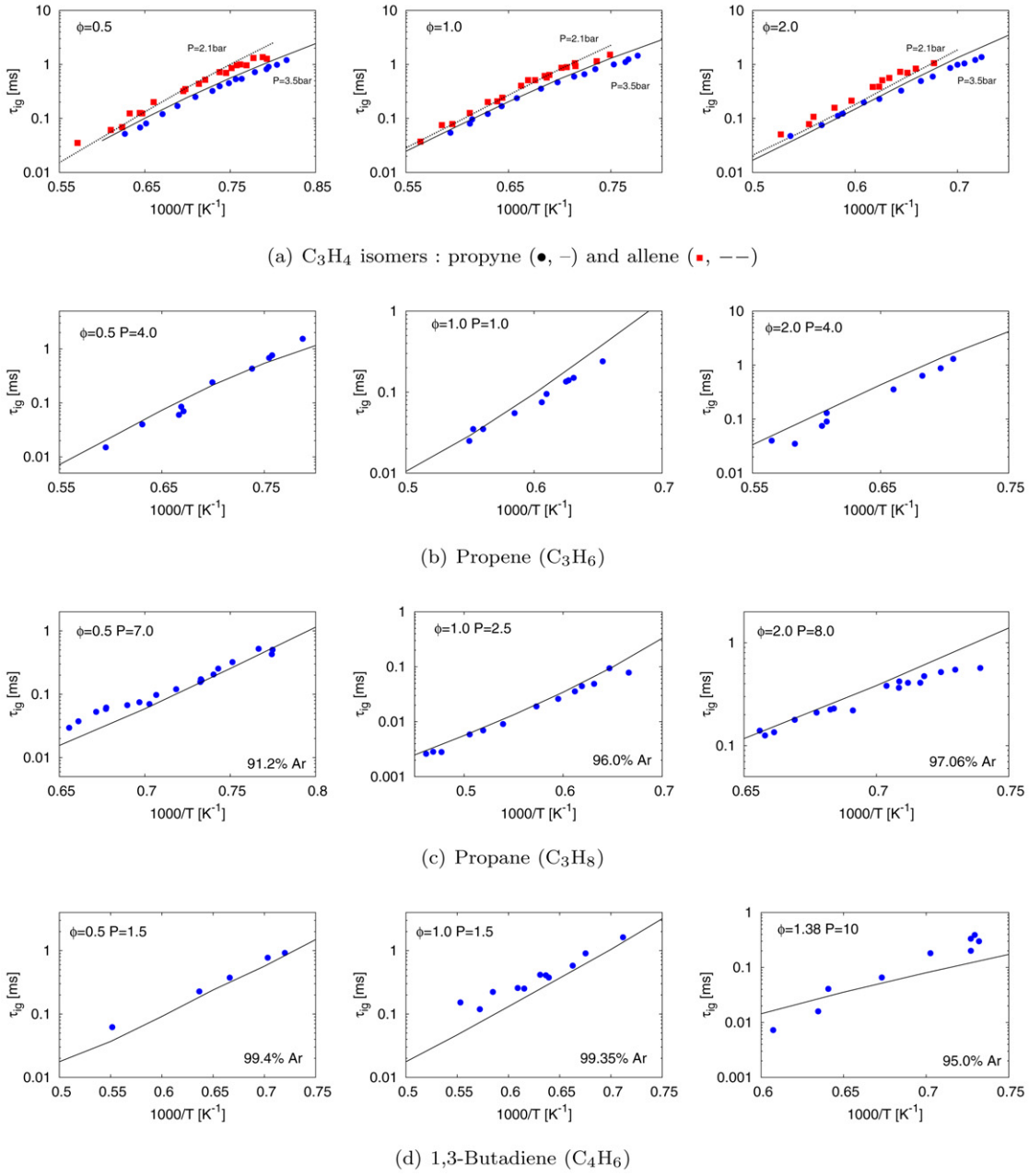

Fig. 2. Ignition delay times for C_3 and C_4 hydrocarbons. References for experimental data are given in the text.

Finally, to ensure that the numerical results were independent of the grid resolution, the simulations were performed using second order central differencing for the convective and diffusion terms with a grid of more than 200 points. Most of the calculations were done at atmospheric pressure and room temperature. Some additional cases were simulated at higher temperatures (up to 450 K) and pressures (up to 25 bar).

3.2.2. Small hydrocarbons

The experimental values for the laminar burning velocities for small hydrocarbon fuels were taken from several data sets including Egolfopoulos et al. [119], Vagelopoulos and Egolfopoulos [120], Hassan et al. [121], Hirasawa et al. [122], Rozenchan et al. [123], Bosschaart and de Goey [124], Jomaas et al. [125], and Kumar et al. [126]. Fig. 5 shows the burning velocities for methane, acetylene, ethylene, and ethane. The overall agreement with experimental data is excellent for all cases except for acetylene. The present mechanism shows significant improvement over the original GRI mechanism v3.0 [23], especially for the combustion of ethylene for which the laminar burning velocity at $\phi = 1.0$ was over-estimated by about 20 $\mathrm{cm\,s^{-1}}$. The present good agreement mainly comes from using more recent rate constants for several key reactions, as presented in the previous sections.

In the case of acetylene, there are only two sets of laminar burning velocities. These two data sets show significant differences for rich conditions (about 35 $\mathrm{cm\,s^{-1}}$ at $\phi = 1.4$), thus rendering the comparison with experimental measurements challenging. The burning velocities predicted for lean mixtures lie right between the two experimental data sets. For stoichiometric to rich mixtures, the flame speeds computed with the current mechanism follow very closely the latest measurements of Jomaas et al. [125] and remain within the experimental uncertainties.

For the three other fuels (methane, ethylene, and ethane), the comparison with experiments is very good. Combustion of both

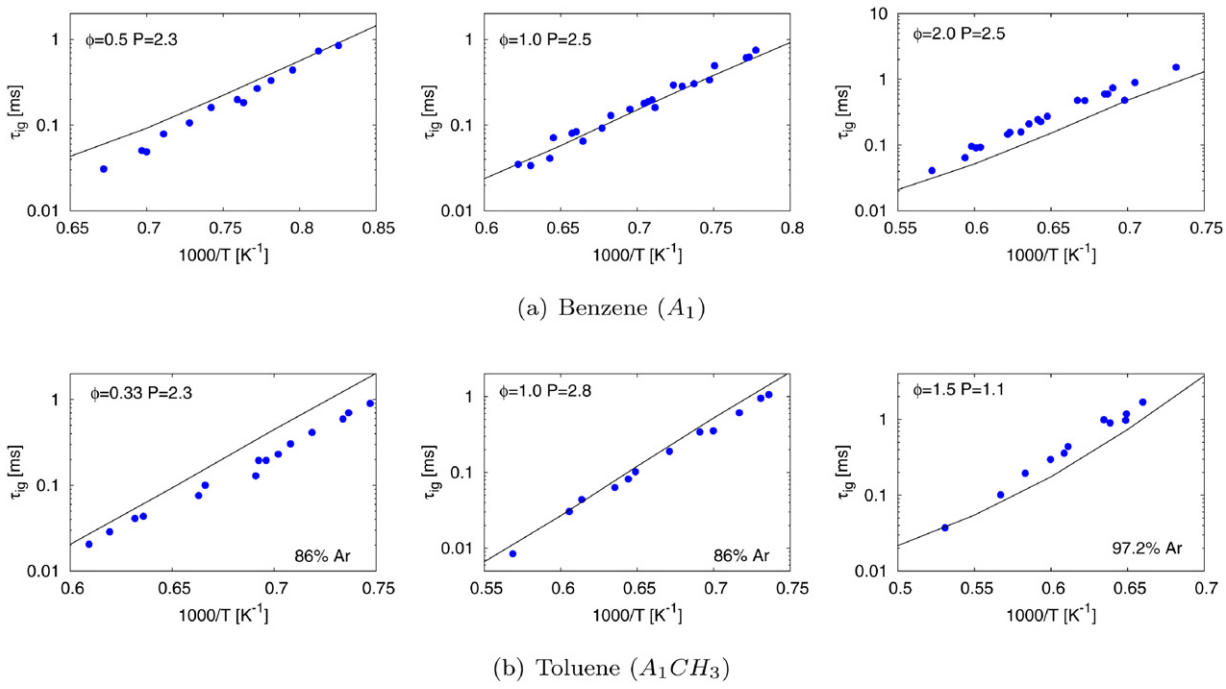

Fig. 3. Ignition delay times for aromatic species. References for experimental data are given in the text.

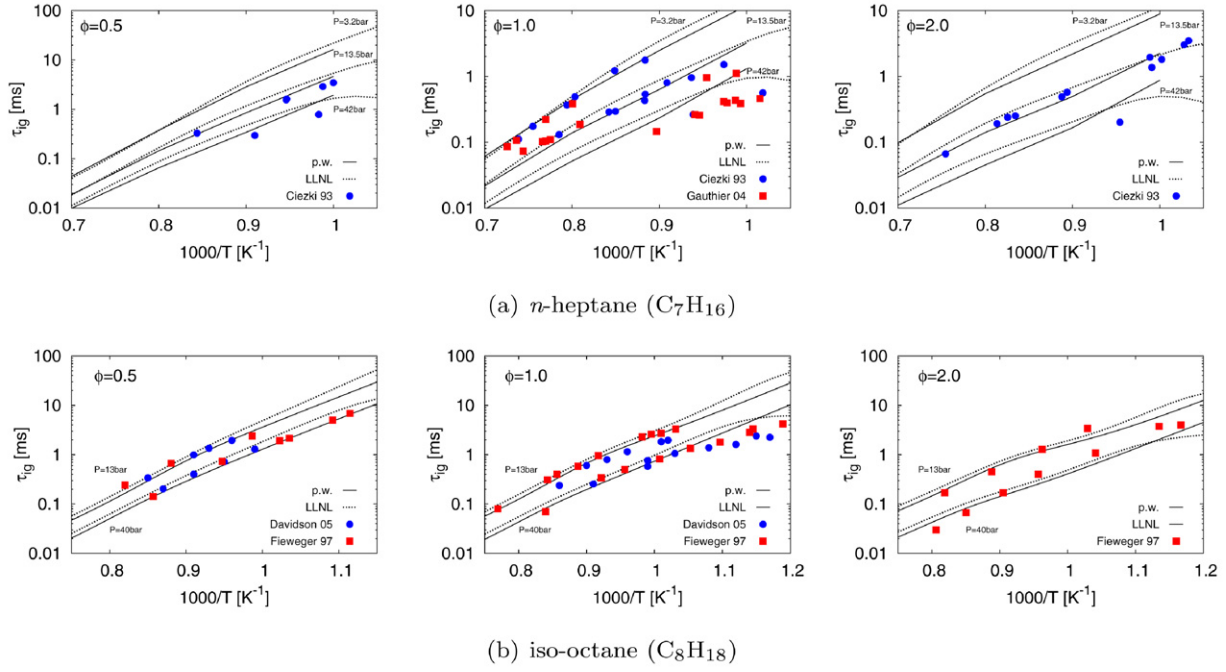

Fig. 4. Ignition delay times for larger alkanes in air. References for experimental data are given in the text.

lean and rich mixtures is correctly represented with the exception of the burning velocities of methane which are slightly overestimated for lean mixtures. The flame speeds of ethane at an equivalence ratio above $\phi = 1.5$ are slightly lower than those measured by Egolfopoulos et al. [119]. However, more recent experimental measurements [124,125] tend to suggest that these values are slightly over-estimated.

Finally, the effect of pressure on the burning velocities for methane, ethylene, and ethane mixtures is correctly represented. The decrease in the burning speed with pressure is well captured for methane flames up to 20 bar.

3.2.3. C_3 and C_4 species

The burning velocity data of C_3 and C_4 hydrocarbons used here are from several experimental sources: Vagelopoulos et al. [127], Davis et al. [128,129], Vagelopoulos and Egolfopoulos [120], Bosschaart and de Goey [124], Jomaas et al. [125], and Saeed and Stone [130]. For reasons mentioned below, the non-linear extrapolated burning velocities of Davis et al. [128,129] were used. With the exception of propyne (18% of O_2 in N_2), all laminar flame speeds were evaluated with air.

Fig. 6 shows the laminar burning velocities of propyne, propene, propane, and butadiene. The calculated values compare very well with the experimental data for the different fuels and the two

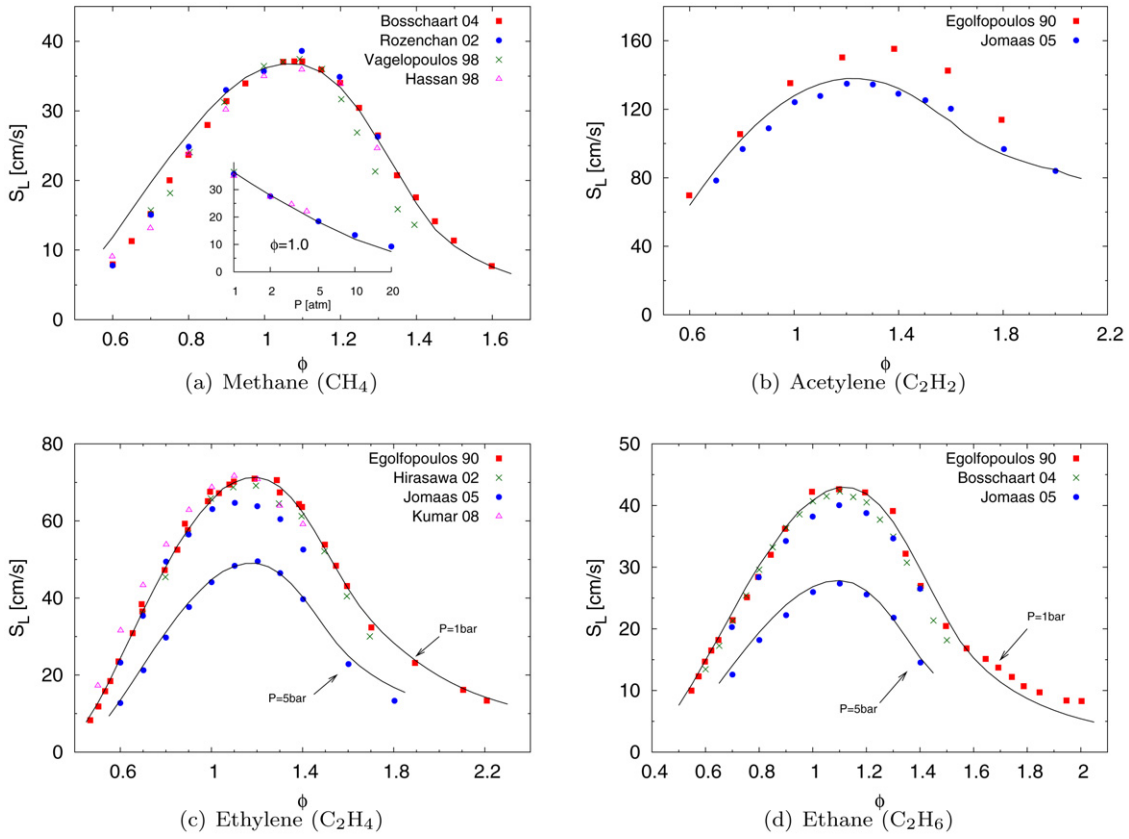

Fig. 5. Laminar burning velocities of small hydrocarbons. References for experimental data are given in the text.

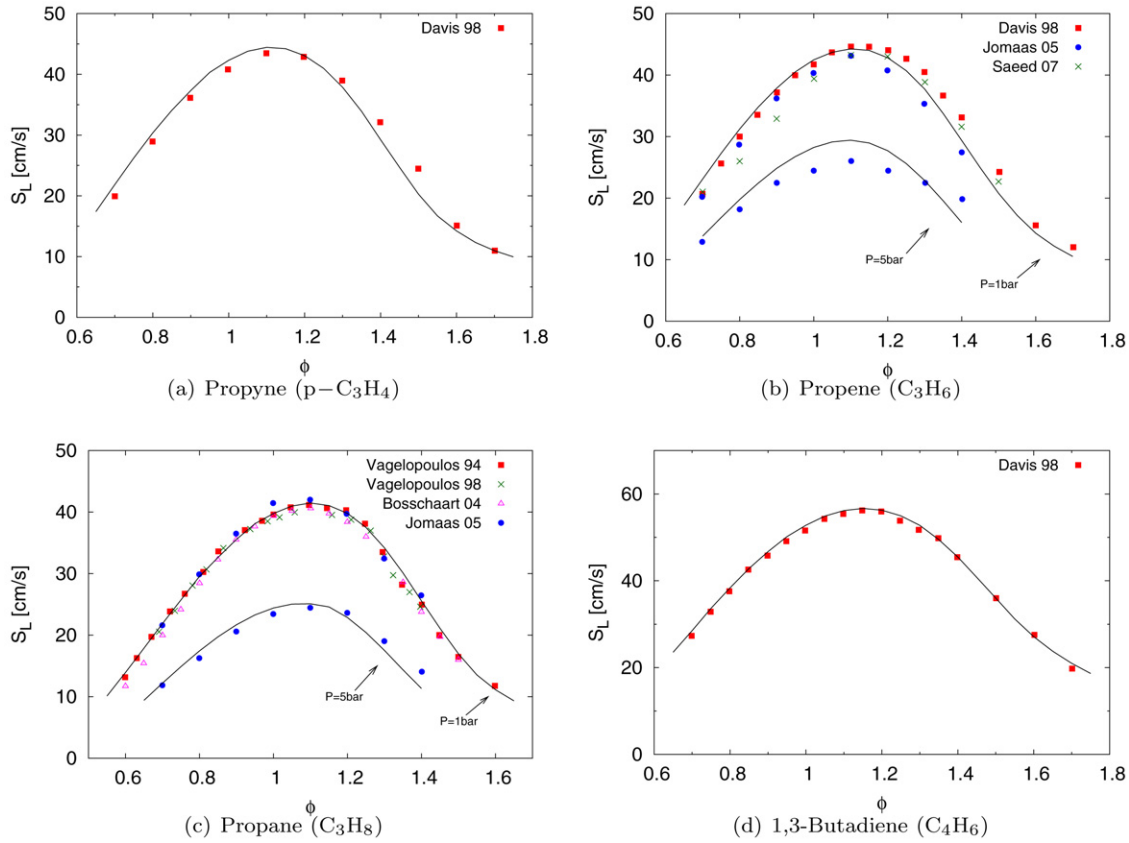

Fig. 6. Laminar burning velocities of C_3 and C_4 hydrocarbons. References for experimental data are given in the text.

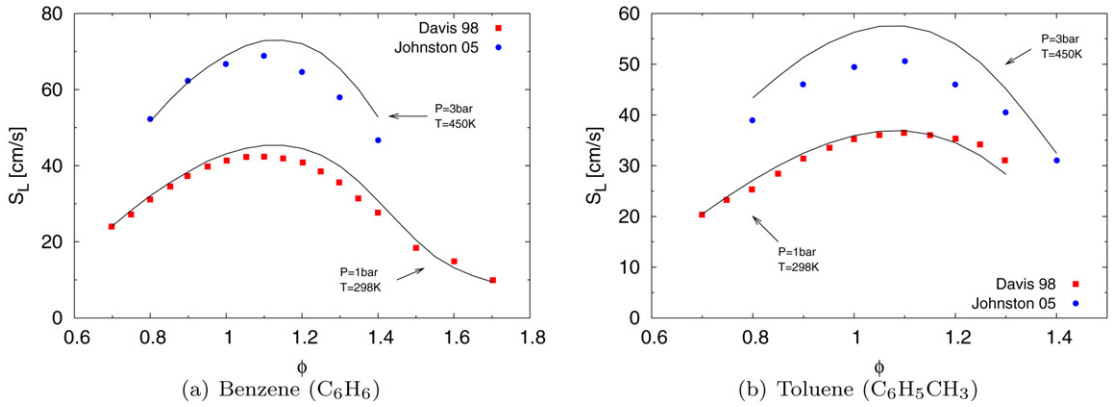

Fig. 7. Laminar burning velocities of aromatic hydrocarbons. References for experimental data are given in the text.

pressures considered. In the case of propene, three data sets are available. Davis and Law [128] estimated the burning velocities obtained using linear and non-linear extrapolation. For this fuel, the non-linear extrapolated burning speed compares more favorably with the other two data sets [125,130] and was therefore used in the comparison. The flame speeds of lean mixtures agree well with the experimental values of Davis and Law [128], while for rich mixtures, the predicted burning speeds compare very well with the more recent data from Saeed and Stone [130]. Given the overall scatter in the experimental data for propene, the comparison of the burning velocities remains very good for both pressures considered.

3.2.4. Aromatics

The burning velocities of benzene and toluene were taken from two data sets. Davis and Law [128] measured the laminar flame speed at atmospheric pressure and room temperature. Johnston and Farrel [131] performed similar measurements at higher pressure ($P = 3$ bar) and higher temperature ($T = 450$ K), more relevant to engine configurations.

Fig. 7 shows the comparison of the calculated laminar burning velocities with the experimental data. The comparison both at low and high pressures is very good for benzene with a slight overprediction for moderately rich mixtures ($1.0 < \phi < 1.5$). The burning velocities of toluene are accurately predicted for atmospheric conditions, but they are overestimated for higher pressures and temperatures. Additional experimental measurements for these conditions and further analysis of the pressure dependence of several reactions relevant to toluene oxidation might be required to explain these discrepancies.

3.2.5. n-Heptane and iso-octane

The laminar burning velocities for *n*-heptane and iso-octane combustion were taken from the results of Davis and Law [128], Bradley et al. [133], Huang and Sung [134], and Kumar et al. [135]. Recently, measurements of the laminar burning velocities for high pressures (from 10 bar up to 25 bar) and higher temperatures (373 K) have been performed by Jerzembeck et al. [132].

Fig. 8 shows the comparison of the calculated laminar flame speeds with the experimental measurements. The burning velocities of *n*-heptane compare very well for both lean and rich mixtures with the data of Davis and Law [128] and Huang and Sung [134]. The more recent data by Kumar et al. [135] show some deviations from the other two data sets and from the current predictions for rich mixtures ($\phi > 1.0$). The calculated burning velocities for iso-octane are in good agreement with experimental measurements for lean mixtures and are slightly smaller for rich mixtures. The increase in the burning velocities due to preheated mixtures ($T = 400$ K) is almost correctly captured for both fuels. However, as was previously mentioned for the case of *n*-heptane at room temperature, the current predicted burning velocities are consistently lower than the experimental data from Kumar et al. [135]. Comparison with older data from Bradley et al. [133] is not conclusive as the burning speed measured at $\phi = 1.0$ is perfectly reproduced by the mechanism while the value measured at $\phi = 0.8$ confirms the data from Kumar et al. [135]. Additional measurements should be considered in order to fully explain these discrepancies.

Finally, Fig. 9 shows the burning velocities predicted for very high pressures from 10 bar to 25 bar [132]. The effects of equivalence ratio and pressure are well captured for *n*-heptane and iso-octane mixtures. However, it should be noticed that the predicted burning velocities are consistently smaller than the measured values for stoichiometric and rich mixtures.

4. Soot precursors in laminar flames

In the previous sections, the present mechanism has been shown to reproduce the ignition delay times and laminar burning velocities of small and large hydrocarbons with good accuracy. To analyze the capabilities of the mechanism to predict the formation of soot precursors, several laminar premixed and diffusion flames are computed. The emphasis is placed on the prediction of soot precursors like acetylene, allene, propyne, and benzene.

4.1. Premixed flat flames

Two laminar premixed flat flames are considered: a rich premixed flame of *n*-heptane/air ($\phi = 1.9$) and a rich premixed flame of iso-octane/air ($\phi = 1.9$). These two flames, close to the sooting limit, were studied experimentally by El Bakali et al. [136], who reported species concentrations and flame temperature. Because of unknown heat losses to the burner by conduction and radiation, the temperature profiles were imposed in the numerical simulations. However, the temperature measurements suffer from significant uncertainties about 5% or ±80 K and ±0.2 mm) due to the use of thermocouples. Furthermore, as the sampling probe is introduced into the flame to measure species concentrations, the flame itself is perturbed. These perturbations typically lead to a mismatch between the measured species concentration and the species concentration predicted by imposing the experimental temperature profile in a numerical simulation [137]. Different strategies have been proposed to account for these discrepancies. The mole fraction profiles can be shifted a few millimeters upstream relative to the unperturbed temperature profile [138]. The temperature profile can be shifted a few millimeters downstream with respect to the unperturbed species concentrations [139]. Finally, the experimental temperature profile can be adjusted to

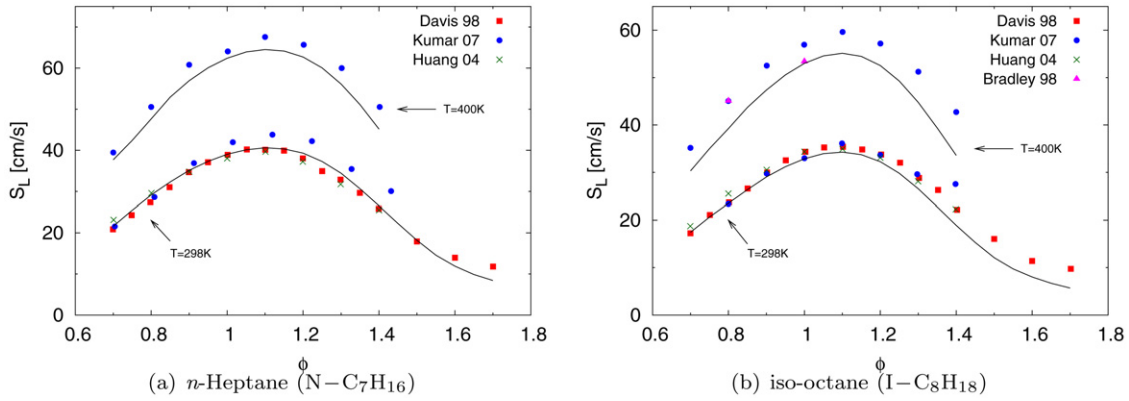

Fig. 8. Laminar burning velocities of *n*-heptane and iso-octane. References for experimental data are given in the text.

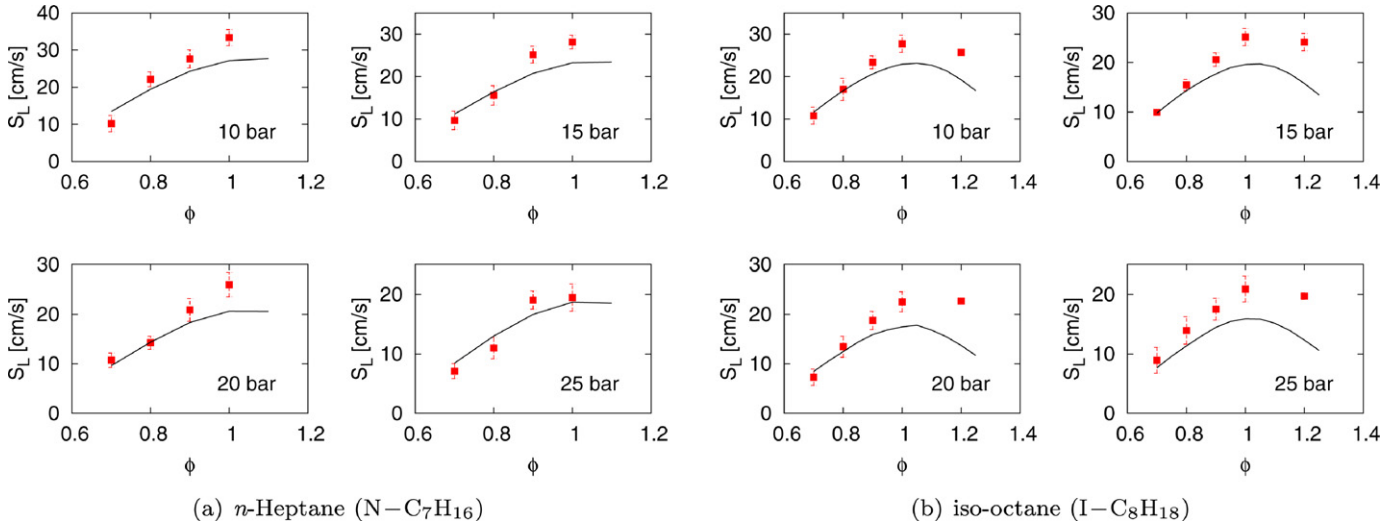

Fig. 9. High pressure laminar burning velocities of *n*-heptane and iso-octane ($T = 373$ K). Experimental data from Jerzembeck et al. [132].

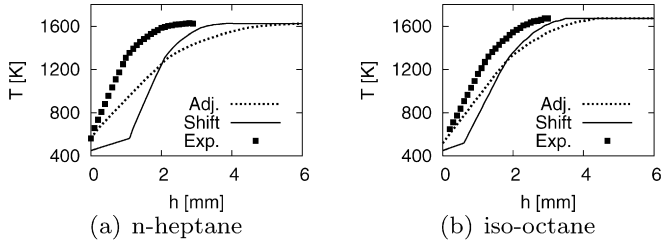

Fig. 10. Temperature profiles used in the numerical simulations of the premixed flames. Symbols: experimental data from El Bakali et al. [136], solid line: shifted temperature profile, dashed line: adjusted profile to match decay of fuel and O_2.

match the decay of important species such as fuel and oxidizer [140]. In the present work, the three methods have been investigated to evaluate the error due to flame modeling on the prediction of soot precursors. The three temperature profiles used in the numerical simulations are shown in Fig. 10 and, the parameters used for these flames are listed in Table 5. These simulations were performed by imposing the mixture composition inside the nozzle and solving convection–diffusion equations to get the mixture composition at the exit plane [96].

The results of the numerical simulations performed with the three different temperature profiles were found to be very similar. Therefore, Figs. 11 and 12 show only the mole fractions of the different species predicted by using the adjusted temperature profiles ("Adj." in Fig. 10). With the temperature profiles adjusted to match the decay of the fuel (*n*-heptane and iso-octane) and the oxidizer,

Table 5
Parameters used for the premixed flames of *n*-heptane, and iso-octane.

Fuel	ϕ	Y_F	Y_{O_2}	Y_{N_2}	v_0 [cm/s]	T_0 [K]	T_{max} [K]
n-heptane	1.9	0.1252	0.2316	0.6432	4.98	450	1628
iso-octane	1.9	0.1465	0.2704	0.5832	4.12	450	1673

the formation of the main products of combustion (CO and CO_2) is correctly reproduced for both flames. The formation of soot precursors like acetylene, allene, propyne, and benzene compares also very well with experimental data.

Table 6 shows the maximum mole fractions of the major species and soot precursors obtained with the three different temperature profiles. The predictions remain very good for any temperature profile as the error for many species is below 20% with the exception of butadiene (C_4H_6) for the iso-octane flame and propene (C_3H_6) for the *n*-heptane flame, whose concentrations are respectively significantly under-predicted and over-predicted. As presented in Table 6, the concentration of acetylene is significantly different for different temperature profiles. This high sensitivity to temperature might explain some of the discrepancies between the predicted and measured acetylene concentrations. The same observation can be made for benzene whose concentration varies by more than a factor of two for the *n*-heptane flame. In light of the strong dependence and uncertainty in temperature, the prediction of the yield of soot precursors remains very satisfactory.

Fig. 13 shows the main pathways leading to the formation of the first aromatic ring in the premixed flames of *n*-heptane and iso-octane. In both flames, the fuel undergoes thermal crack-

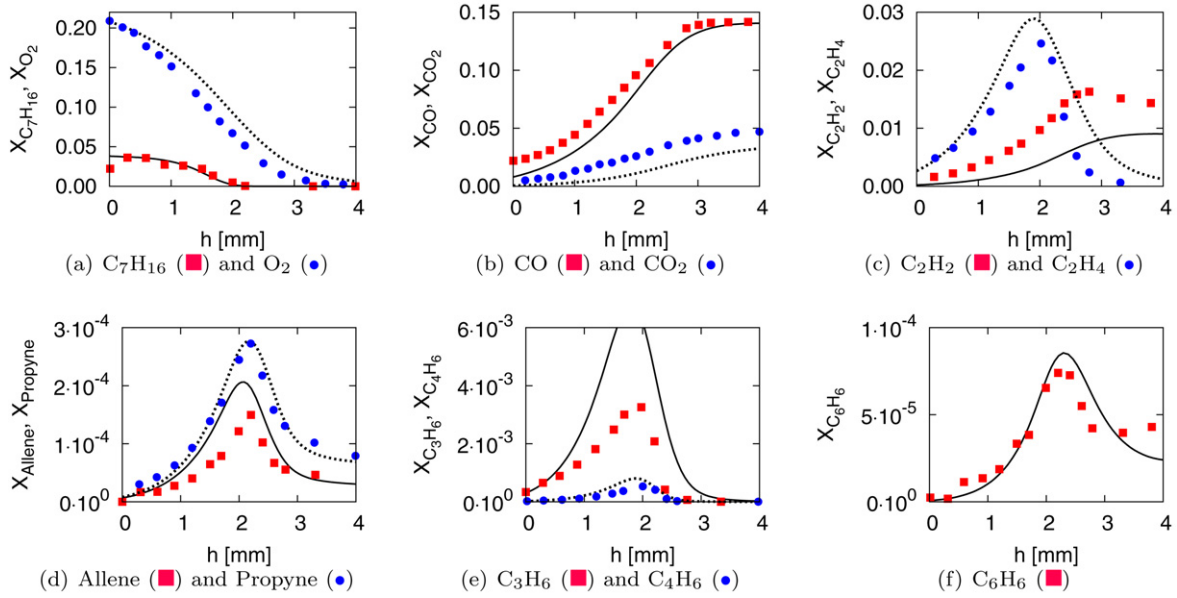

Fig. 11. Mole fractions of main species and soot precursors for the rich *n*-heptane premixed flame. Experimental data from El Bakali et al. [136], lines are simulations performed with the adjusted temperature profile (Fig. 10(a)).

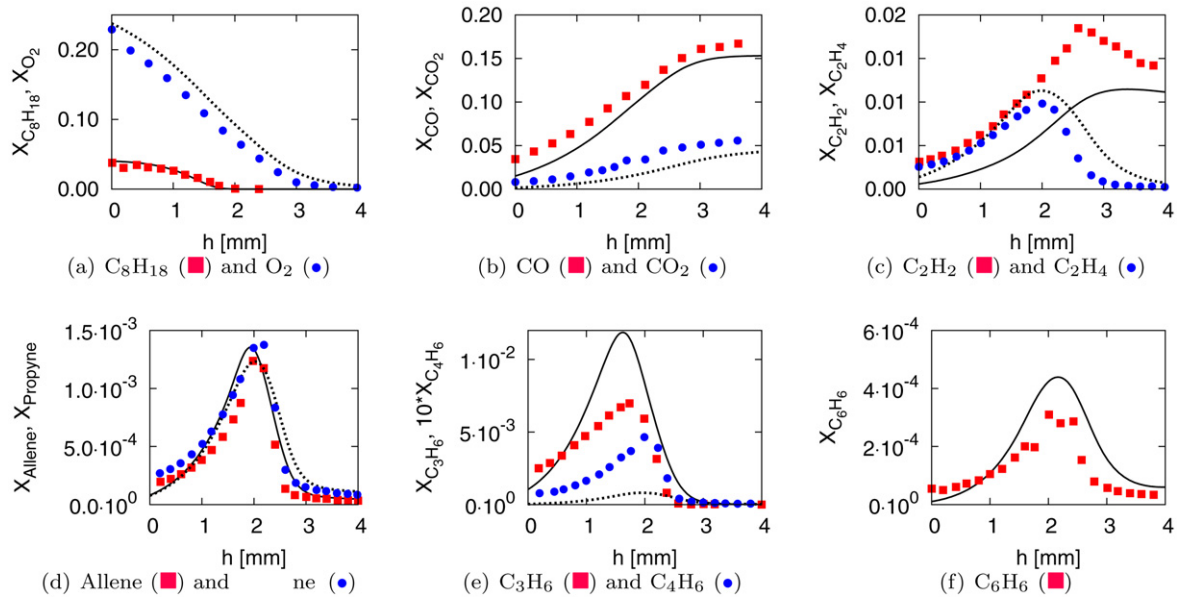

Fig. 12. Mole fractions of main species and soot precursors for the rich iso-octane premixed flame. Experimental data from El Bakali et al. [136], lines are simulations performed with the adjusted temperature profile (Fig. 10(b)).

Table 6
Maximum species mole fractions for the simulations performed with the different temperature profiles (Fig. 10). Italic: error of more than 20%, bold: error of more than 100%.

(a) *n*-Heptane					(b) iso-Octane				
Species	Numerical simulations			Experiments Ref. [136]	Species	Numerical simulations			Experiments Ref. [136]
	Exp.	Shift	Adj.			Exp.	Shift	Adj.	
CH_4	1.5e−2	1.5e−2	1.6−2	1.4e−2	CH_4	2.5e−2	*2.8e−2*	*2.8e−2*	2.2e−2
C_2H_2	*1.1e−2*	1.4e−2	*9.1e−3*	1.6e−2	C_2H_2	*1.2e−2*	1.5e−2	*1.2e−2*	1.8e−2
C_2H_4	2.1e−2	2.6e−2	2.9e−2	2.5e−2	C_2H_4	9.5e−3	1.1e−2	1.1e−2	9.8e−3
C_2H_6	1.5e−3	1.8e−3	*2.0e−3*	1.6e−3	C_2H_6	*3.6e−3*	*4.1e−3*	*4.3e−3*	2.9e−3
a-C_3H_4	1.5e−4	*2.6e−4*	*2.1e−4*	1.5e−4	*a*-C_3H_4	1.3e−3	*1.6e−3*	1.4e−3	1.2e−3
p-C_3H_4	2.4e−4	*3.9e−4*	2.8e−4	2.7e−4	*p*-C_3H_4	1.2e−3	1.5e−3	1.2e−3	1.4e−3
C_3H_6	*4.6e−3*	*6.0e−3*	**6.8e−3**	3.3e−3	C_3H_6	*9.8e−3*	*1.1e−2*	*1.1e−2*	7.0e−3
C_3H_8	*1.9e−4*	2.4e−4	3.1e−4	2.6e−4	C_3H_8	9.7e−5	1.2e−4	1.2e−4	9.6e−5
C_4H_6	4.9e−4	5.8e−4	*8.1e−4*	5.3e−4	C_4H_6	**7.5e−5**	**1.0e−4**	**1.4e−4**	4.6e−4
C_6H_6	*5.7e−5*	*1.3e−4*	8.0e−5	7.4e−5	C_6H_6	*4.0e−4*	*5.6e−4*	*4.3e−4*	3.1e−4

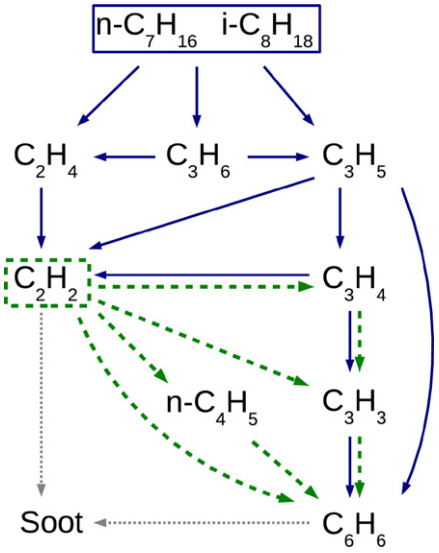

Fig. 13. Main pathways leading to the formation of the first aromatic ring for the alkane flames (solid lines) and the acetylene flame (dashed line).

ing mostly through beta-scission reactions. During this process, smaller and smaller molecules are formed, ultimately leading to ethylene. Later, ethylene molecules are converted into acetylene. Another byproduct of the fuel decomposition is the formation of C_3 species (the C_3H_4 isomers, a-C_3H_5, and C_3H_6) in large quantities. In these alkane flames, the C_3H_4 isomers are formed mainly from the direct decomposition of the fuel and not from smaller hydrocarbons. Then, through H-abstraction reactions, propargyl radicals are rapidly formed from the C_3H_4 isomers. Finally, the first aromatic ring is formed from the recombination of propargyl radicals or the reaction of propargyl and allyl radicals. While present in the mechanism, the formation of benzene/fulvene from acetylene addition on C_4H_5 radicals was not found to be important for these two alkane flames.

4.2. Counterflow diffusion flames

Two counterflow diffusion flames are considered. The first flame is an acetylene/air diffusion flame by Pels Leusden and Peters [141,142] with a lean premixed flame ($\phi = 0.63$) on the oxidizer side. The second flame is a n-heptane/air diffusion flame by Berta et al. [143] with a very rich premixed flame on the fuel side ($\phi = 15$). Contrary to the premixed flames simulated previously, the temperature profiles were not imposed in the current simulations of the diffusion flames. The maximum of the temperature profile occurs away from the two burners, and heat losses to the burners by conduction should not be significant. The simulations were performed with a simple model to account for radiation heat losses [144].

Figs. 14 and 15 show the mole fraction profiles for the main species and the soot precursors. The decay of the fuels (C_2H_2 and C_7H_{16}) and the oxidizer is correctly represented for both flames, as is the formation of the main products of combustion (CO and CO_2). The predictions for the different soot precursors compare favorably with the experimental data, with the exception of the ethylene and the C_3H_4 isomers profiles for the acetylene flame which are underpredicted by a factor of two. As mentioned previously, the concentration of propyne and allene were found very sensitive to the rates of the H-abstraction reactions leading to the formation of propargyl radicals. As these rates were estimated, it is not surprising to observe some discrepancies in the prediction of these species. However, the concentration of benzene was found insensitive to those rates. For the acetylene diffusion flame, the profiles for C_2H_2, CO, CO_2, and C_6H_6 appear to be shifted towards the fuel nozzle. This small shift is most likely due to buoyancy effects not included in the simulation [145]. In the case of the n-heptane diffusion flame, the mole fraction of benzene is overestimated by a factor of two. The concentration of benzene was measured with two different experimental techniques (filled squares and circles) [143]. Given the large scatter between these two measurements, the overall agreement with the experimental data for the benzene profile remains reasonable.

Fig. 13 shows the main pathways leading to the formation of the first aromatic ring in the diffusion flames of n-heptane and acetylene. For the n-heptane diffusion flame, the C_3H_4 isomers are formed from the direct decomposition of the fuel as was observed in the premixed flame previously presented. On the other hand, for the acetylene diffusion flame, the C_3H_4 isomers are formed from the reaction of methyl radicals with acetylene present in large quantity. In both cases, the propargyl and allyl radicals react with one another to form benzene. Then, toluene molecules are formed

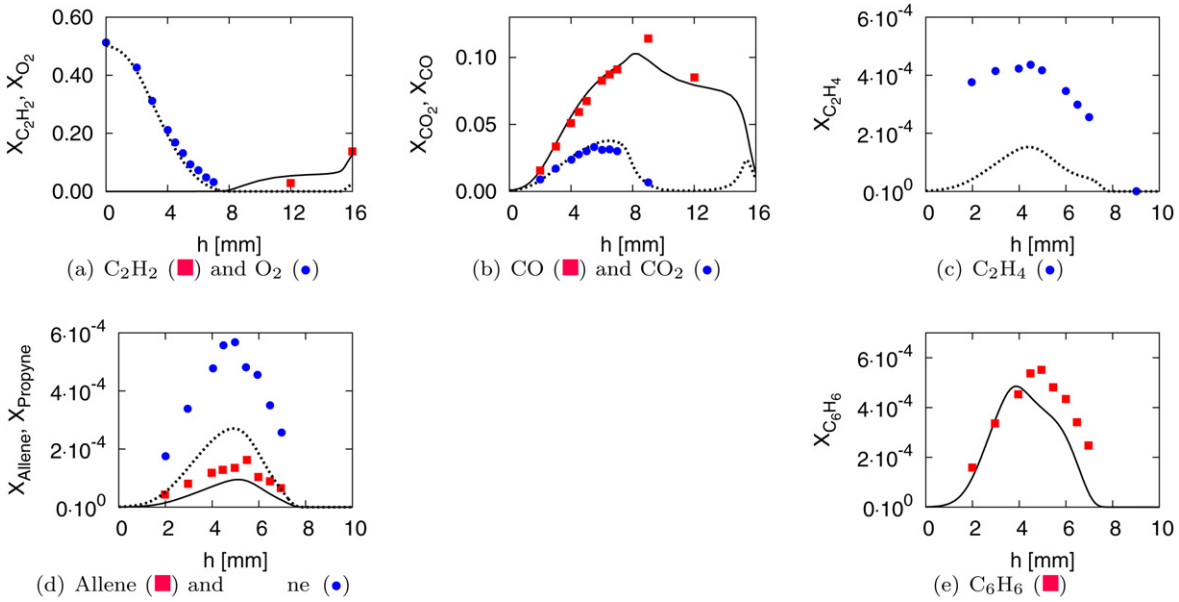

Fig. 14. Mole fractions of main species and soot precursors for the acetylene diffusion flame. Experimental data from Pels Leusden and Peters [141,142].

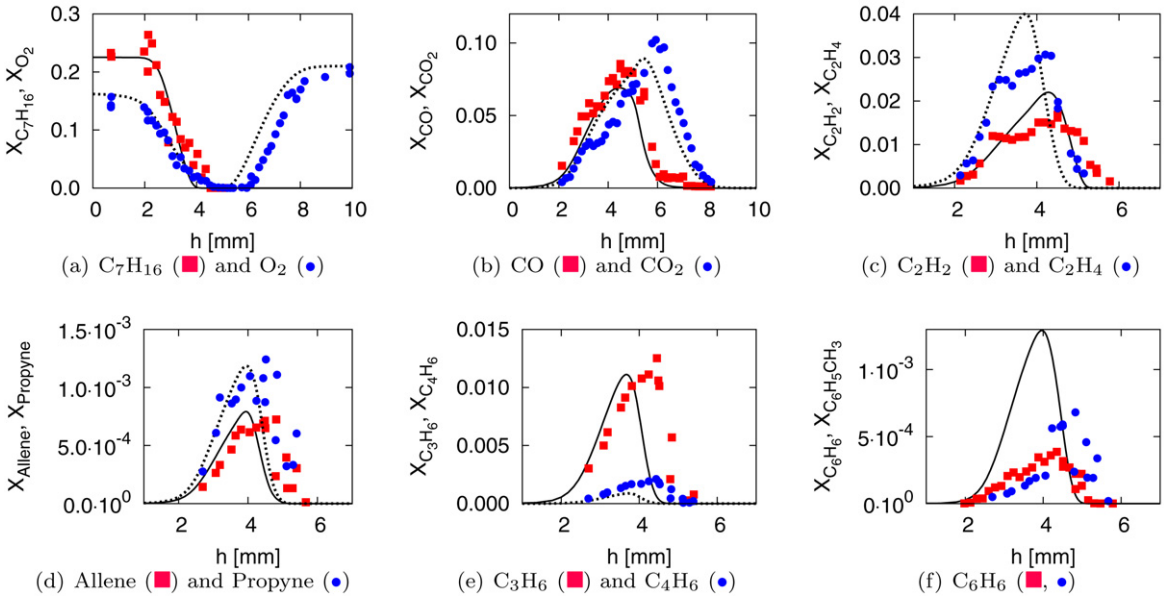

Fig. 15. Mole fractions of main species and soot precursors for the *n*-heptane diffusion flame. Experimental data from Berta et al. [143].

by addition of methyl radicals on benzene or phenyl rings. In contrary to the alkane flames, the normal butadienyl radical (n-C_4H_5) is found very important to the formation of the first aromatic ring. This species is formed from the reaction of acetylene with vinyl radicals. Later, benzene molecules are formed from the addition of acetylene onto the butadienyl radical. While not important for the alkane flames, this pathway contributes up to 40% of the total rate of benzene formation for the acetylene diffusion flame.

These four laminar flames show that the mode of combustion (premixed or diffusion) might have little influence on the pathways leading to the formation of soot precursors such as benzene. However, the chemical structure of the fuel affects significantly the mechanisms of benzene formation by enabling or disabling entire reaction pathways. A detailed representation of the chemistry of soot precursors is thus required to properly predict the formation of benzene in various flames with different fuels.

5. Conclusions

A chemical mechanism has been developed for the high temperature combustion of engine relevant fuels. In this development, a particular emphasis has been placed on the chemistry of soot precursors like acetylene, the C_3H_4 isomers (allene and propyne), propene, butadiene, and benzene. Finally, the mechanism has been extended to include the chemistry relevant to aromatic combustion (benzene and toluene) and the combustion of larger alkanes like *n*-heptane and iso-octane.

The full mechanism has been validated extensively against ignition delay times and laminar burning velocities over a large range of equivalence ratios and pressures. The comparison with experimental measurements is very good in almost all cases. Then, the mechanism has been used in the simulation of a series of laminar rich premixed and diffusion flames. The profiles of the main species as well as the soot precursors compare favorably with experimental data. However, additional experimental measurements in laminar premixed and diffusion flames with aromatic fuels (benzene and toluene) would be useful for further validation of the chemical model.

The chemical steps responsible for the formation of benzene and other soot precursors were analyzed in these flames. It was shown that the reaction pathways leading to the formation of C_3 and C_4 species (and then benzene) can be significantly different different flames with different fuels. An accurate description of the mechanisms of decomposition of the fuel and the formation of soot precursors is necessary for an accurate description of soot formation.

Acknowledgments

The authors gratefully acknowledge funding by the US Department of Energy within the ASC program, from SERDP, and from the Air Force Office of Scientific Research.

Supplementary material

The online version of this article contains additional supplementary material.

Please visit DOI: 10.1016/j.combustflame.2008.12.007.

References

[1] H.R. Zhang, E.G. Eddings, A.F. Sarofim, Proc. Combust. Inst. 31 (2007) 401–409.
[2] M. Colket, T. Edwards, S. Williams, N. Cernansky, D. Miller, F. Egolfopoulos, P. Lindstedt, K. Seshadri, F. Dryer, C. Law, D. Friend, D. Lenhert, H. Pitsch, A. Sarofim, M. Smooke, W. Tsang, Development of an experimental database and kinetic models for surrogate jet fuels, in: 45th AIAA Aerospace Sciences Meeting and Exhibit, Reno, NV, January 8–11, 2007, p. 0770.
[3] D.B. Olson, J.C. Pickens, Combust. Flame 62 (1985) 43–60.
[4] C.S. McEnally, L.D. Pfefferle, Combust. Flame 148 (2007) 210–222.
[5] J. Appel, H. Bockhorn, M. Frenklach, Combust. Flame 121 (2000) 122–136.
[6] F. Mauss, B. Trilken, J. Breitbach, N. Peters, in: H. Bockhorn (Ed.), Soot Formation in Combustion—Mechanism and Models, Springer-Verlag, 1994, pp. 325–349.
[7] C.A. Schuetz, M. Frenklach, Proc. Combust. Inst. 29 (2002) 2307–2314.
[8] M. Frenklach, H. Wang, Proc. Combust. Inst. 23 (1991) 1559–1566.
[9] J.A. Miller, S.J. Klippenstein, J. Phys. Chem. A 107 (2003) 7783–7799.
[10] A. D'Anna, J.H. Kent, Combust. Flame 132 (2003) 715–722.
[11] J.P. Senosiain, S.J. Klippenstein, J.A. Miller, J. Phys. Chem. A 17 (2006) 5772–5781.
[12] NIST computational chemistry comparison and benchmark database—Release 14, http://srdata.nist.gov/cccbdb.
[13] NIST chemistry webbook, http://webbook.nist.gov/chemistry.
[14] J.A. Seetula, Phys. Chem. Chem. Phys. 1 (1999) 4727–4731.
[15] S.J. Klippenstein, J.A. Miller, J. Phys. Chem. A 109 (2005) 4285–4295.
[16] S.E. Wheeler, W.D. Allen, H.F. Schaefer, J. Chem. Phys. 121 (2004) 8800–8813.
[17] H. Wang, K. Brezinsky, J. Phys. Chem. A 102 (1998) 1530–1541.
[18] J.H. Kiefer, R.S. Tranter, H. Wang, A.F. Wagner, Int. J. Chem. Kinet. 33 (2001) 834–845.
[19] I.V. Tokmakov, L.V. Moskaleva, M.C. Lin, Int. J. Chem. Kinet. 36 (2003) 139–151.

[20] C. Xu, X. You, M. Braun-Unkhoff, M. Naumann, P. Frank, Th. Just, H. Wang, Shock tube pyrolysis of 1,2-diiodobenzene—Kinetics of H atom production in high-temperature thermal decomposition of ortho-benzyne, in: 6th International Conference on Chemical Kinetics, Gaithersburg, USA, 2005.
[21] A. Fattahi, S.R. Kass, J.F. Liebman, M.A.R. Matos, M.S. Miranda, V.M.F. Morais, J. Am. Chem. Soc. 127 (2005) 6116–6122.
[22] S.G. Davis, A.V. Joshi, H. Wang, F. Egolfopoulos, Proc. Combust. Inst. 30 (2005) 1283–1292.
[23] G.P. Smith, D.M. Golden, F. Frenklach, N.W. Moriarty, B. Eiteneer, M. Goldenberg, C.T. Bowman, R.K. Hanson, S. Song, W.C.J. Gardiner, V.V. Lissianski, Z. Qin, http://www.me.berkeley.edu/grimech/.
[24] B. Eiteneer, M. Frenklach, Int. J. Chem. Kinet. 35 (2003) 391–414.
[25] A. Laskin, H. Wang, C.K. Law, Int. J. Chem. Kinet. 32 (2000) 589–614.
[26] G. Blanquart, H. Pitsch, J. Phys. Chem. A 111 (2007) 6510–6520.
[27] H.J. Curran, P. Gaffuri, W.J. Pitz, C.K. Westbrook, Combust. Flame 114 (1998) 149–177.
[28] H.J. Curran, P. Gaffuri, W.J. Pitz, C.K. Westbrook, Combust. Flame 129 (2002) 253–280.
[29] A. Burcat, B. Ruscic, Ideal gas thermochemical database with updates from active thermochemical tables, ftp://ftp.technion.ac.il/pub/supported/aetdd/thermodynamics/ (2008).
[30] L.B. Harding, Y. Georgievskii, S.J. Klippenstein, J. Phys. Chem. A 109 (2005) 4646–4656.
[31] A. Laskin, H. Wang, Chem. Phys. Lett. 303 (1999) 43–49.
[32] H. Wang, Int. J. Chem. Kinet. 33 (2001) 698–706.
[33] J.A. Miller, S.J. Klippenstein, Phys. Chem. Chem. Phys. 6 (2004) 1192–1202.
[34] J.P. Senosiain, S.J. Klippenstein, J.A. Miller, J. Phys. Chem. A 17 (2005) 6045–6055.
[35] J.P. Senosiain, S.J. Klippenstein, J.A. Miller, J. Phys. Chem. A 21 (2006) 6960–6970.
[36] B. Ludwig, W. Brandt, G. Friedrichs, F. Temps, J. Phys. Chem. A 110 (2006) 3330–3337.
[37] L.B. Harding, S.J. Klippenstein, Y. Georgievskii, Proc. Combust. Inst. 30 (2005) 985–993.
[38] H.J. Curran, Int. J. Chem. Kinet. 38 (2006) 250–275.
[39] T.L. Nguyen, L. Vereecken, X.J. Hou, M.T. Nguyen, J. Peeters, J. Phys. Chem. A 33 (2005) 7489–7499.
[40] J.A. Miller, S.J. Klippenstein, S.H. Robertson, Proc. Combust. Inst. 28 (2000) 1479–1486.
[41] R.S. Zhu, Z.F. Xu, M.C. Lin, J. Chem. Phys. 120 (2004) 6566–6573.
[42] A. Chakraborty, Y. Zhao, H. Lin, D.G. Truhlar, J. Chem. Phys. 124 (2006) 044315-1–044315-14.
[43] L.N. Krasnoperov, J. Michael, J. Phys. Chem. A 26 (2004) 5643–5648.
[44] H. Carstensen, A. Dean, Proc. Combust. Inst. 30 (2005) 995–1003.
[45] D. Baulch, C. Bowman, C. Cobos, R. Cox, T. Just, J. Kerr, M. Pilling, D. Stocker, J. Troe, W. Tsang, R.W. Walker, J. Warnatz, J. Phys. Chem. Ref. Data 34 (2005) 757–1397.
[46] M.A. Oehlschlaeger, D.F. Davidson, R.K. Hanson, W. Tsang, H. Hippler, J. Troe, Proc. Combust. Inst. 30 (2005) 1119–1127.
[47] W. Tsang, R.F. Hampson, J. Phys. Chem. Ref. Data 15 (1986) 1087–1279.
[48] Y. Hidaka, Y. Henmi, T. Ohonishi, T. Okuno, Combust. Flame 130 (2002) 62–82.
[49] N.M. Marinov, W.J. Pitz, C.K. Westbrook, M.J. Castaldi, S.M. Senkan, Combust. Sci. Technol. 116 (1996) 211–287.
[50] S. Davis, C. Law, H. Wang, J. Phys. Chem. A 103 (1999) 5889–5899.
[51] J.A. Miller, J.P. Senosiain, S.J. Klippenstein, Y. Georgievskii, J. Phys. Chem. A 112 (39) (2008) 9429–9438.
[52] M. Blitz, M. Beasley, M. Pilling, S. Robertson, Phys. Chem. Chem. Phys. 2 (2000) 805–812.
[53] H.G. Yu, J.T. Muckerman, J. Phys. Chem. A 109 (2005) 1890–1896.
[54] S. Stoliarov, V. Knyazev, I. Slagle, J. Phys. Chem. A 106 (2002) 6952–6966.
[55] L.B. Harding, S.J. Klippenstein, Y. Georgievskii, J. Phys. Chem. A 111 (2007) 3789–3801.
[56] S.J. Miller, J.A. Klippenstein, J. Phys. Chem. A 107 (2003) 2680–26920.
[57] D. Hahn, S. Klippenstein, J. Miller, Faraday Discuss. 119 (2001) 79–100.
[58] B. Ceursters, H. Nguyen, J. Peeters, M. Nguyen, Chem. Phys. 262 (2000) 243–252.
[59] S.J. Miller, J.A. Klippenstein, J. Phys. Chem. A 109 (2005) 4285–4295.
[60] J.P. Senosiain, S.J. Klippenstein, J. Miller, Proc. Combust. Inst. 31 (2007) 185–192.
[61] S.J. Miller, J.A. Klippenstein, S.H. Robertson, J. Phys. Chem. A 104 (2000) 7525–7536.
[62] A.A. Shestov, K.V. Popov, I.R. Slagle, V.D. Knyazev, Chem. Phys. Lett. 408 (2005) 339–343.
[63] Z.M. Djurisic, Detailed kinetic modeling of benzene and toluene oxidation at high temperatures, Master's thesis, University of Delaware, Newark, DE (November 1999).
[64] Detailed kinetic modeling of benzene and toluene oxidation at high temperatures, http://diesel.me.berkeley.edu/~zoran/publications/2000_MS_Thesis.
[65] X. Zhong, J.W. Bozzelli, Int. J. Chem. Kinet. 29 (1997) 893–913.
[66] X. Zhong, J.W. Bozzelli, J. Phys. Chem. 20 (1998) 3537–3555.
[67] M.A. Oehlschlaeger, D.F. Davidson, R.K. Hanson, Combust. Flame 147 (2006) 195–208.
[68] K. Roy, Kinetische Untersuchung zur Hochtemperaturpyrolyse und -oxidation von Cyclopentadien und Cyclopentadienyl mit Hilfe der Stosswellentechnik, Ph.D. thesis, Stuttgart University, Germany (1999).
[69] V.D. Knyazev, I.R. Slagle, J. Phys. Chem. A 106 (2002) 5613–5617.
[70] M. Lu, J.A. Mulholland, Chemosphere 42 (2001) 625–633.
[71] P. Lindstedt, L. Maurice, M. Meyer, Faraday Discuss. 119 (2002) 409–432.
[72] C.S. McEnally, L.D. Pefferle, B. Atakan, K. Kohse-Hinghaus, Prog. Energy Combust. Sci. 32 (2006) 247–294.
[73] Y. Murakami, T. Saejung, C. Ohashi, N. Fujii, Chem. Lett. 12 (2003) 1112–1113.
[74] V.V. Kislov, A.M. Mebel, J. Phys. Chem. A 111 (2007) 9532–9543.
[75] R.G. Butler, I. Glassman, Proc. Combust. Inst. 32 (1) (2009) 395–402.
[76] H. Wang, M. Frenklach, J. Phys. Chem. 98 (1994) 11465–11489.
[77] J.P. Senosiain, J.A. Miller, J. Phys. Chem. A 111 (2007) 3740–3747.
[78] Y. Georgievskii, J.A. Miller, S.J. Klippenstein, Phys. Chem. Chem. Phys. 9 (2007) 4259–4268.
[79] I.V. Tokmakov, M.C. Lin, J. Phys. Chem. A 106 (2002) 11309–11326.
[80] T. Seta, M. Nakajima, A. Miyoshi, J. Phys. Chem. A 110 (2006) 5081–5090.
[81] H.Y. Zhang, J.T. McKinnon, Combust. Sci. Technol. 107 (1995) 261–300.
[82] D. Hodgson, H.Y. Zhang, M.R. Nimlos, J.T. McKinnon, J. Phys. Chem. A 105 (2001) 4316–4327.
[83] T.L. Nguyen, J. Peeters, L. Vereecken, J. Phys. Chem. A 111 (2007) 3836–3859.
[84] Z.F. Xu, M.C. Lin, J. Phys. Chem. A 110 (2006) 1672–1677.
[85] Y. Murakami, K. Mitsui, K. Naito, T. Itoh, T. Kobayashim, N. Fujii, Shock Waves 13 (2003) 149–154.
[86] S.J. Klippenstein, L.B. Harding, Y. Georgievskii, Proc. Combust. Inst. 31 (2007) 221–229.
[87] M.A. Oehlschlaeger, D.F. Davidson, R.K. Hanson, J. Phys. Chem. A 110 (2006) 6649–6653.
[88] J. Jones, G.B. Backsay, J.C. Mackie, J. Phys. Chem. A 101 (1997) 7105–7113.
[89] V. Vasudevan, D.F. Davidson, R.K. Hanson, Proc. Combust. Inst. 30 (2005) 1155–1163.
[90] Y.M. Choi, W.S. Xia, J. Park, M.C. Lin, J. Phys. Chem. A 104 (2000) 7030–7035.
[91] W.S. Xia, M.C. Lin, Phys. Chem. Chem. Phys. 2 (2000) 5566–5570.
[92] V.V. Kislov, N.I. Islamova, A.M. Kolker, S.H. Lin, A.M. Mebel, J. Chem. Theory Comput. 1 (2005) 908–924.
[93] N.W. Moriarty, M. Frenklach, Proc. Combust. Inst. 28 (2000) 2563–2568.
[94] J. Aguilera-Iparraguirre, W. Klopper, J. Chem. Theory. Comput. 3 (2007) 139–145.
[95] P. Pepiot-Desjardins, H. Pitsch, Combust. Flame 154 (1–2) (2008) 67–81.
[96] G. Blanquart, P. Pepiot-Desjardins, H. Pitsch, Assessing uncertainties in numerical simulations of simple reacting flows using the flamemaster code, Combust. Theory Model. (2009), in preparation.
[97] D.J. Seery, C.T. Bowman, Combust. Flame 14 (1970) 37–47.
[98] Y. Hidaka, K. Hattori, T. Okuno, K. Inami, T. Koike, Combust. Flame 107 (1996) 401–417.
[99] M.J.A. Rickard, J.M. Hall, E.L. Petersen, Proc. Combust. Inst. 30 (2005) 1915–1923.
[100] Y. Hidaka, T. Nishimori, K. Sato, R. Henmi, Y. Okuda, K. Inami, T. Higashihara, Combust. Flame 117 (1999) 755–776.
[101] D.C. Horning, A study of the high temperature autoignition and thermal decomposition of hydrocarbons, Ph.D. thesis, Stanford University (2001).
[102] J. de Vries, J.M. Hall, S.L. Simmons, M.J.A. Rickard, D.M. Kalitan, E.L. Petersen, Combust. Flame 150 (2007) 137–150.
[103] H. Curran, J.M. Simmie, P. Dagaut, D. Voisin, M. Cathonnet, Proc. Combust. Inst. 26 (1996) 613–620.
[104] Z. Qin, H. Yang, W.C.J. Gardiner, Combust. Flame 124 (2001) 246–254.
[105] C.J. Brown, G.O. Thomas, Combust. Flame 117 (1999) 861–870.
[106] A. Burcat, A. Lifshitz, K. Scheller, G.B. Skinner, Proc. Combust. Inst. 13 (1970) 745–755.
[107] C. Libby, D.F. Davidson, R.K. Hanson, A shock tube study of the oxidation of 1,3-butadiene, in: 42nd AIAA Aerospace Sciences Meeting and Exhibit, Reno, NV, January 5–8, 2004, p. 1322.
[108] R. Fournet, J.C. Bauge, F. Battin-Leclerc, Int. J. Chem. Kinet. 31 (1999) 361–379.
[109] H. Wang, M. Frenklach, Combust. Flame 110 (1997) 173–221.
[110] A. Burcat, C. Snyder, T. Brabbs, Ignition delay times of benzene and toluene with oxygen in argon mixtures, Tech. Rep. TM-87312, NASA (1986).
[111] P. Dagaut, G. Pengloan, A. Ristori, Phys. Chem. Chem. Phys. 4 (2002) 1846–1854.
[112] H.K. Ciezki, G. Adomeit, Combust. Flame 93 (1993) 421–433.
[113] B.M. Gauthier, D.F. Davidson, R.K. Hanson, Combust. Flame 139 (2004) 300–311.
[114] K. Fieweger, R. Blumenthal, G. Adomeit, Combust. Flame 109 (1997) 599–619.
[115] D.F. Davidson, B.M. Gauthier, R.K. Hanson, Proc. Combust. Inst. 30 (2005) 1175–1182.
[116] H. Li, Z.C. Owens, D.F. Davidson, R.K. Hanson, Int. J. Chem. Kinet. 40 (2007) 189–198.
[117] P. Middha, B. Yang, H. Wang, Proc. Combust. Inst. 29 (2002) 1361–1369.
[118] P. Middha, H. Wang, Combust. Theory Model. 9 (2005) 353–363.
[119] F.N. Egolfopoulos, D.L. Zhu, C.K. Law, Proc. Combust. Inst. 23 (1990) 471–478.
[120] C.M. Vagelopoulos, F.N. Egolfopoulos, Proc. Combust. Inst. 27 (1998) 513–519.

[121] M.I. Hassan, K.T. Aung, G.M. Faeth, Combust. Flame 115 (1998) 539–550.
[122] T. Hirasawa, C.J. Sung, A. Joshi, Z. Yang, H. Wang, C.K. Law, Proc. Combust. Inst. 29 (2002) 1427–1434.
[123] G. Rozenchan, D.L. Zhu, C.K. Law, S.D. Tse, Proc. Combust. Inst. 29 (2002) 1461–1469.
[124] K.J. Bosschaart, L.P.H. de Goey, Combust. Flame 136 (2004) 261–269.
[125] G. Jomaas, X.L. Zheng, D.L. Zhu, C.K. Law, Proc. Combust. Inst. 30 (2005) 193–200.
[126] K. Kumar, G. Mittal, C.J. Sung, C.K. Law, Combust. Flame 153 (2008) 343–354.
[127] C.M. Vagelopoulos, F.N. Egolfopoulos, C.K. Law, Proc. Combust. Inst. 23 (1994) 1341–1347.
[128] S.G. Davis, C.K. Law, Combust. Sci. Technol. 140 (1998) 427–449.
[129] C.K. Davis, S.G. Law, H. Wang, Proc. Combust. Inst. 27 (1998) 305–312.
[130] K. Saeed, R. Stone, J. Energy Inst. 80 (2007) 73–82.
[131] R.J. Johnston, J.T. Farrell, Proc. Combust. Inst. 30 (2005) 217–224.
[132] S. Jerzembeck, N. Peters, P. Pepiot-Desjardins, H. Pitsch, Combust. Flame 156 (2) (2009) 292–301.
[133] D. Bradley, R.A. Hicks, M. Lawes, C.G.W. Sheppard, R. Woolley, Combust. Flame 115 (1998) 126–144.
[134] Y. Huang, C. Sung, J. Eng, Combust. Flame 139 (2004) 239–251.
[135] K. Kumar, J.E. Freeh, C.J. Sung, Y. Huang, J. Prop. Power 23 (2007) 428–436.
[136] A.E. Bakali, J.L. Delfau, C. Vovelle, Combust. Sci. Technol. 140 (1998) 69–91.
[137] A.T. Hartlieb, B. Atakan, K. Kohse-Hoeinghaus, Combust. Flame 121 (2000) 610–624.
[138] A. Tregrossi, A. Ciajolo, R. Barbella, Combust. Flame 117 (1999) 553–561.
[139] A.E. Bakali, J.L. Delfau, C. Vovelle, Combust. Flame 118 (1999) 381–398.
[140] H.R. Zhang, E.G. Eddings, A.F. Sarofim, Combust. Sci. Technol. 179 (2007) 61–89.
[141] C. Pels Leusden, N. Peters, Proc. Combust. Inst. 28 (2000) 2619–2625.
[142] C. Pels Leusden, Experimentelle und theoretische Untersuchung der Russbildung in laminaren Gegenstromdiffusionsflammen, Ph.D. thesis, RWTH Aachen (2001).
[143] P. Berta, S.K. Aggarwal, I.K. Puri, Combust. Flame 145 (2006) 740–764.
[144] W.L. Grosshandler, A narrow-band model for radiation calculations in a combustion environment, Tech. Rep. 1402, NIST (1993).
[145] R. Seiser, L. Truett, D. Trees, K. Seshadri, Proc. Combust. Inst. 27 (1998) 649–657.